Functional development of the enteric nervous system in larval zebrafish

BS-MS Thesis

Submitted to
Indian Institute of Science Education and Research Pune
In partial fulfilment of the requirements for the
BS-MS Dual Degree Programme

By
Rajlakshmi Sawale
20151087

Indian Institute of Science Education and Research Pune
Dr. Homi Bhabha Road,
Pashan, Pune 411008, INDIA.

March, 2020

Supervisor: Dr. Ethan Scott
Queensland Brain Institute, Australia

Certificate

This is to certify that this dissertation entitled **"Functional development of the enteric nervous system in larval zebrafish"** towards the partial fulfilment of the BS-MS dual degree programme at the Indian Institute of Science Education and Research, Pune represents study carried out by Rajlakshmi Sawale at The University of Queensland, Australia under the supervision of Dr. Ethan Scott, Associate Professor, Queensland Brain Institute during the academic year 2019-2020.

Rajlakshmi Sawale
20151087
IISER Pune

Dr. Ethan Scott
Associate Professor
Queensland Brain Institute

Committee:
Supervisor: Dr. Ethan Scott
TAC: Dr. Raghav Rajan

This thesis is dedicated to my parents and my sister for being the most supportive and loving family one can hope for.

Declaration

I hereby declare that the matters embodied in the report entitled **"Functional development of the enteric nervous system in larval zebrafish"** are the results of the work carried out by me at The University of Queensland, Australia, under the supervision of Dr. Ethan Scott and the same has not been submitted elsewhere for any other degree.

Rajlakshmi Sawale
20151087
5th-year BS-MS
IISER Pune

Acknowledgments

I would like to thank my supervisor, Dr. Ethan Scott for his valuable guidance throughout the tenure of this project. I want to thank my co-supervisor and mentor Dr. Gilles Vanwalleghem, for teaching me the techniques crucial for this project and guiding me throughout every stage of this project. I thank them for their thoughtful feedback and constant encouragement which has helped me gain experience and move forward. I would like to thank all the lab members, Gilles, Leandro, Emmanuel, Maya, Itia, Lena, Rebecca, Sebastian, Tessa, Anahita and Justine for their feedback, all the wonderful lunch table discussions and fun lab outings. I am thankful to all the amazing people around me, old friends and new friends that I have met during my stay in Australia.

Abstract

The enteric nervous system (ENS) controls various functions of the gastrointestinal tract and interacts with the gut microbiome. It communicates with the brain in multiple ways, through endocrine and immune signalling, and direct neuronal signalling via the vagus nerve. Patients with psychiatric (anxiety, depression) or neurological disorders (autism spectrum disorders, Parkinson's disease) often show gastrointestinal comorbidities. Furthermore, several correlative studies have implicated the gut-brain axis in effects on behaviour and cognition. From these studies, the ENS is the interface between gut, microbiome and brain, however the causal links between the different factors remain elusive. This provides the motivation to study the functional development of the ENS in zebrafish larvae and investigate the influence of the gut microbiome on its development. This might prove to be the first step leading to the dramatic effects on behaviour that are observed at later time points. In this project, we started out with the first step wherein we characterized the functional development of the ENS in wildtype zebrafish larvae. We employed light-sheet microscopy to image the activity of the ENS in 2-7 days post fertilization larvae using a genetically encoded calcium indicator, GCaMP6s. We examined the properties of growth of the ENS network, gained insights into the developmental trajectory it follows and characterised the patterns of activity it exhibits, which correspond to the waves of peristalsis that it brings about. This is the first-ever study of its kind and serves as the first step towards understanding the functional development of the ENS.

Table of contents

List of figures

List of tables

List of abbreviations

dpf = Days post fertilization

ENS = Enteric Nervous System

CNS = Central Nervous System

PNS = Peripheral Nervous System

SPIM = Selective Plane Illumination Microscopy

seqNMF = Sequential Non-negative Matrix Factorization

t-SNE = t-distributed Stochastic Neighbour Embedding

SBFSEM = Serial Block Face Scanning Electron Microscopy

Chapter 1
Introduction

1.1 Background

1.1.1 The nervous system

The nervous system is mainly divided into two parts: the central nervous system (CNS) and the peripheral nervous system (PNS) (Figure 1.1) (Rao and Gershon, 2016). The brain and spinal cord form the central nervous system, whereas the peripheral nervous system is a network of nerves and ganglia that arise from the CNS and spread throughout the body. Sensory information (represented in yellow) from the periphery is transmitted to the CNS via neurons of the dorsal root ganglia and cranial nerve ganglia. This information is processed and integrated by the brain to send motor outputs (represented in blue) via efferent nerves either to the skeletal muscles which coordinate body movements, and are under conscious control, or to the autonomous nervous system, which consists of three further divisions: sympathetic, parasympathetic and enteric. The autonomic nervous system has control over involuntary bodily functions such as maintaining cardiovascular control, breathing, bowel and bladder control.

1.1.2 The enteric nervous system (ENS)

The enteric nervous system (ENS) is a complex, interconnected network of series of ganglionated plexi with multiple subtypes of neurons and glia that innervates the entire length of the gastrointestinal tract. The human ENS consists of about 200-600 million neurons, similar in number to the spinal cord, it is the largest component of the peripheral nervous system (Furness et al., 2014). The ENS comprises not only the ganglia that line the gastrointestinal organs, but also the nerve fibres connecting these ganglia and the nerve fibres that innervate the muscle layer surrounding the gut lumen, blood vessels and other tissues. While the CNS innervates sympathetic and parasympathetic ganglia, it does not directly innervate most of the enteric neurons. Additionally, the enteric neuronal circuitry comprises intrinsic primary afferent neurons that can sense the local environmental stimuli, integrate information and initiate motor actions by themselves. The ENS, therefore, stands out from the rest of the nervous system in possessing both sensory and motor properties and can function independently (Rao and Gershon, 2016).

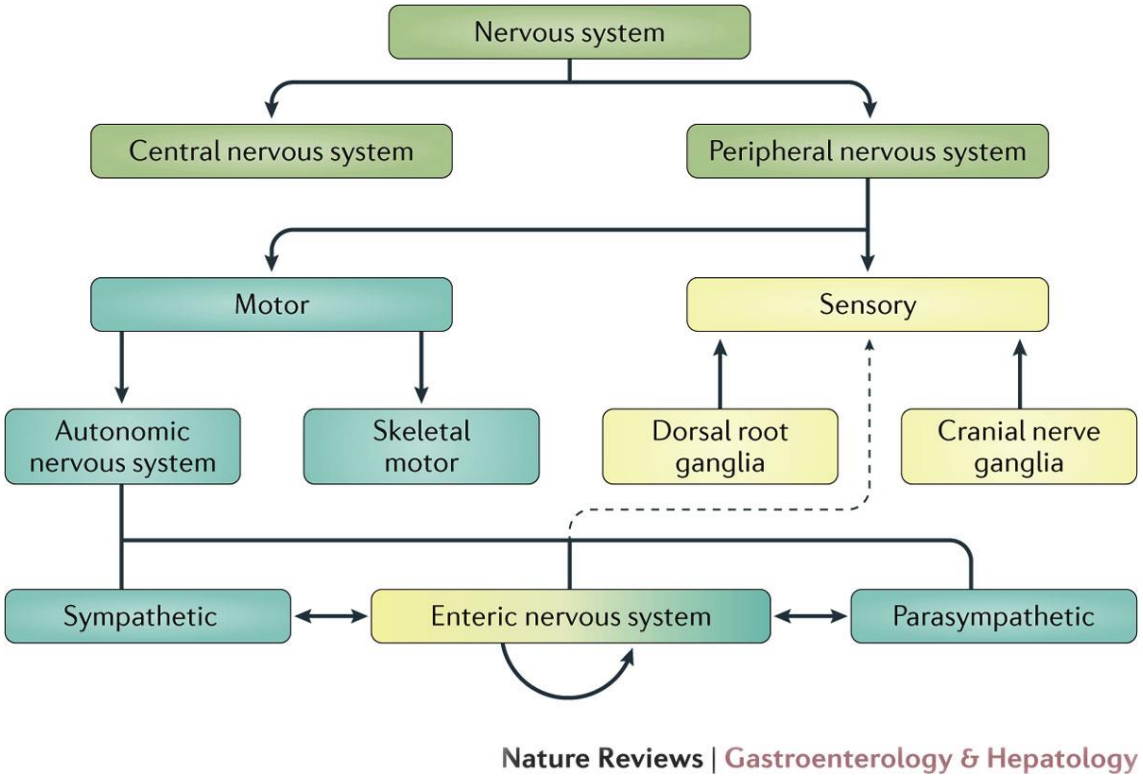

Figure 1.1: Relationship between the enteric nervous system (ENS) and the other components of the nervous system. The components involved in the flow of sensory information are represented in yellow whereas the motor components are represented in blue. The ENS possesses both sensory and motor properties and the bidirectional communication between the ENS and the CNS via the PNS is represented by a dotted line. (Adapted from Rao and Gershon, 2016).

However, even though the ENS can function independently without inputs from the CNS, in practice, it rarely does. In fact, it is in constant communication with the CNS. There is an integrated bidirectional flow of information between the CNS and the ENS through multiple ways such as endocrine signalling, immune signalling and neuronal signalling via the vagus nerve (Han et al., 2018; Kaelberer et al., 2018). The two-way communication involves local enteric reflexes, reflexes passing through sympathetic ganglia and other neural connections from the gut to the CNS and vice versa (Figure 1.2) (Furness, 2014). The CNS and the ENS along with sympathetic neural circuits bring about functions of digestion. The neural reflex circuits within the ENS sense the physiological status of the gut and based on this, regulate important functions such as driving gut motility, hormone secretion, local blood flow, nutrient uptake and maintenance of homeostasis (Furness et al., 2014).

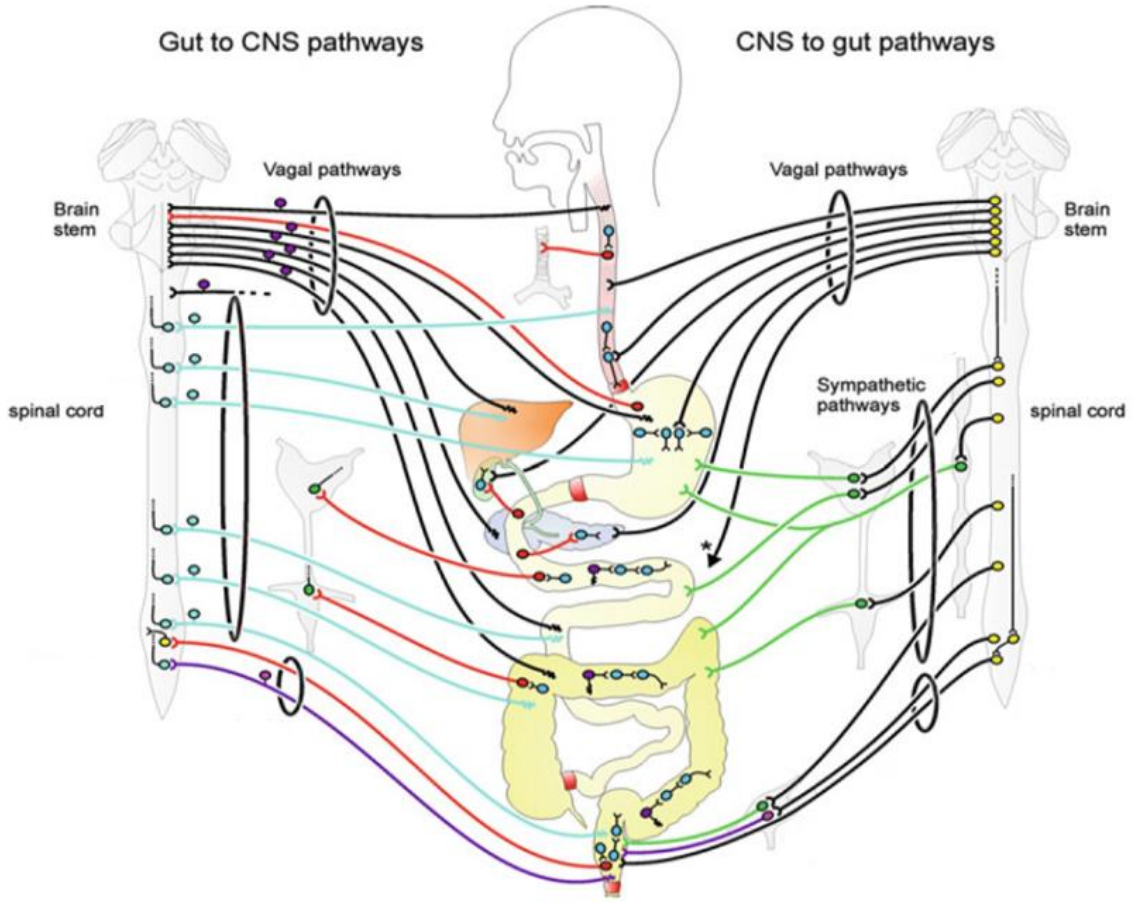

Figure 1.2: Two way communication between the enteric nervous system and the central nervous system via the rest of the peripheral nervous system. The left part of the figure shows connections from the ENS to CNS and the other organs whereas the connections from the CNS are shown in the right part. Within the gastrointestinal tract, the ENS circuits are represented with motor components in blue and sensory components in purple. The components of the CNS that transmit information to the gut are shown in yellow. Information from the CNS to the ENS and other gastrointestinal organs is passed through vagal and sympathetic pathways (right). The sympathetic components receive information from both CNS (green, right) as well as the ENS (red, left). (Adapted from Furness 2014)

The gut epithelium contains numerous enteroendocrine cells with several receptors on their surface that allow them to detect a variety of signals from the gut lumen, encode this information using various transmitters and pass it on to the rest of the body as secretion of hormones or to the nervous system as neurotransmitters (Ye et al., 2017). The complex ensemble of the gut connectome along with enteroendocrine cells thus provides a spatio-temporal signal sensing mechanism

and a real time modulatory feedback of the enteroendocrine function. Enteric neurons innervate the muscle that coats the gastrointestinal tract and are coordinated by the enteric reflex circuits to drive gut motility (Hao et al., 2016). Another important neural pathway is the vagus nerve which is involved in both afferent as well as efferent roles as it innervates the gut (Mayer, 2011).

1.1.3 Gut-microbiota brain axis

All animals live in close contact with microorganisms and act as hosts for numerous microbial communities inevitably on every surface of their body, starting from the skin to the surface lining the gastrointestinal tract. Humans and microbes have a mutualistic relationship where they are constantly coevolving, exerting selective pressure on each other and influencing the physiology of one another. Host-microbiota interactions in the gut are known to play a profound role in host health and development (Lynch and Pedersen, 2016). In the last two decades, multiple studies have shown that gut microbiota influences the gut-brain axis. Several studies have implicated complex two-way communication between the gut microbes and the central nervous system via direct interactions, as well as parallel signalling mechanisms (Ma et al., 2019). The brain has a strong hold over the composition and function of the gut microbiome via control over gut motility, intestinal permeability, intestinal secretions, and by secreting hormones that directly affect microbial gene expression in the intestinal lumen. On the other hand, the microbiome also modulates the CNS via neuroimmune, neuroendocrine pathways, often involving the vagus nerve (Singh et al., 2016; Wang et al., 2014; Bravo et al., 2011). This is achieved by microbial metabolites generated by microbes using the substrates from the food ingested by the host (Matsumoto et al., 2012). These metabolites and other signalling factors from the microbes interact with the cells within the gut connectome (enteroendocrine cells and enterochromaffin cells) and the intestinal mucosa (Furness et al., 2014). This information is further relayed to the brain via the various pathways involved in the gut-brain axis (Figure 1.3). Moreover, microbes can also produce neuroactive molecules that can directly affect the CNS. (Lyte, 2013; Asano et al., 2012; Barrett et al., 2012).

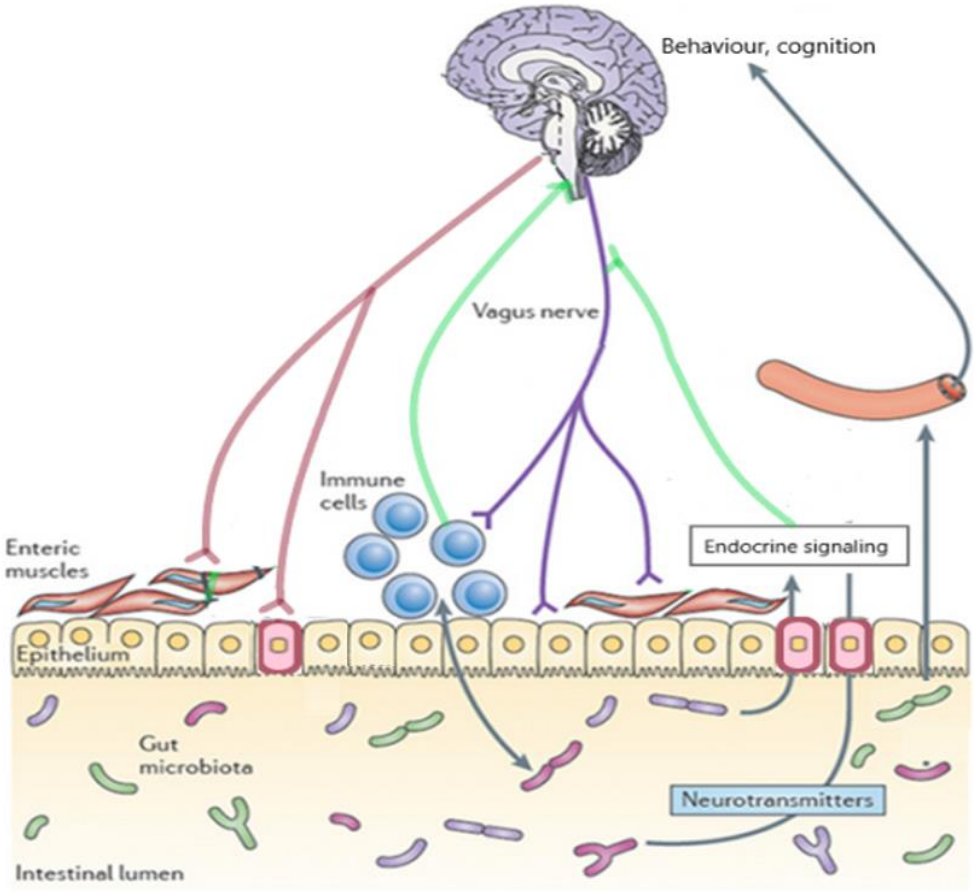

Figure 1.3: The gut-brain axis. A schematic representing the various pathways (enteroendocrine cells shown in red, immune pathways, neural pathways, neuroactive chemicals) through which the gut microbiome communicates with and influences the central nervous system. (Modified from: Petschow et al., 2013)

1.1.4 Gut-brain axis in mental health

Several correlative studies have suggested that, in addition to its digestive and neuroendocrine functions, the gut-microbiome axis influences behaviour and cognition at a global level (Desbonnet et al., 2014). The first ever study in this regard was by Sudo et al., where they showed that absence of normal gut microbiome in early life has effects on stress responsiveness and this can be partially rescued by early reintroduction of conventional gut microbiota (Sudo et al., 2004). Following this, several studies have also investigated the associated neurochemical changes, such as changes in serotonin receptor levels in the hippocampus (Neufeld et al., 2011; Borre et al., 2014) amongst others, further implying that the gut microbiome employs several ways to exert an influence over the brain and behaviour. Further, many

preclinical and clinical studies have gone ahead and implicated the gut microbiome in mental health (McDonald et al., 2018; Cryan and Dinan., 2012; Valles-Colomer et al., 2019). For instance, reintroducing microbes in the gut of germ-free animals affect their anxiety-like (Bravo et al., 2011; Desbonnet et al., 2010; Bercik et al., 2011; Crumeyrolle-Arias et al., 2014; Hsiao et al., 2013; Desbonnet et al., 2015) or depression-like behaviours (Kelly et al., 2016; Desbonnet et al., 2008; Arseneault-Bréard et al., 2012; Zheng et al., 2016). Patients with psychiatric disorders like anxiety, depression or neurological disorders like autism spectrum disorder, Parkinson's disease are often observed to have gastrointestinal comorbidities such as irritable bowel syndrome (IBS), constipation, abdominal pain or diarrhea (Mertsalmi et al., 2017; Adams et al., 2011; McElhanon et al., 2014; Chaidez et al., 2014). In summary, many converging studies provide growing evidence of a potential role for the gut microbiome in multiple disorders affecting the nervous system apart from just influencing its normal development and function.

1.2 Rationale

1.2.1 Insights from the background

Most of the studies that address the interplay between the gut microbiome, brain and behaviour are mostly correlative. The causality still remains elusive and needs to be addressed in order to gain firm insights into the link between these three factors. In this entire scenario, based on recent studies, the ENS seems to be acting as an interface between the gut microbiome and its effect on brain and behaviour (Figure 1.4). Given the close proximity between the microbiome and the ENS, it follows that there is a strong interplay between the two. Studies in rodents have shown that the gut microbiota influence the development and function of the ENS (Obata and Pachnis, 2016). All the dramatic effects of gut microbiota on behaviour and cognition that are observed provide the motivation to study how things start out in first place. Given that the ENS acts as an interface, it makes sense to delve into investigating the structural and functional development of the enteric nervous system and the effects of gut microbiome on it.

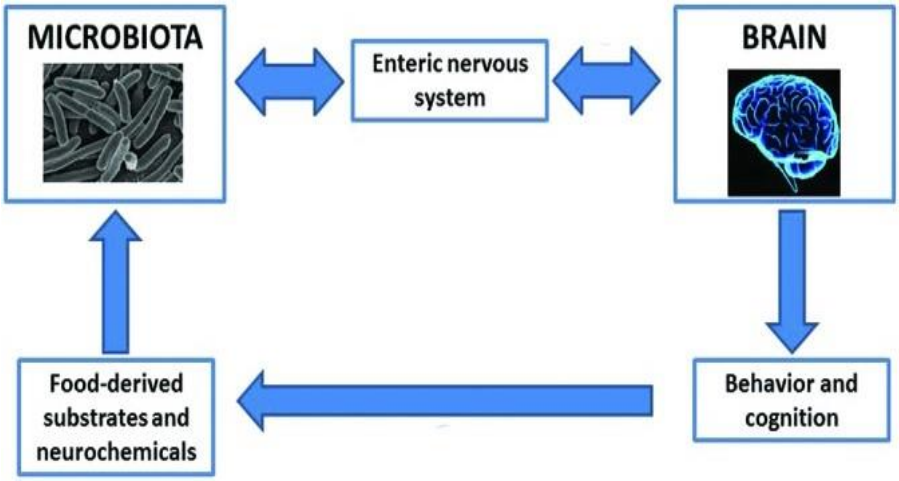

Figure 1.4: ENS as an interface: Microbiota can produce neuroactive chemicals using the substrates available from the food ingested by the host. The sensory receptors of the host ENS interact with these neurochemicals, communicate this information and influence the rest of the nervous system and the brain. This ultimately may cause an altered behaviour. However, the brain also controls the microbial composition by causing the release of certain neurochemicals into the intestinal lumen (represented by the two-way arrows). (Adapted from Lyte et al., 2014)

1.2.2 The big picture

The long-term goal of this study is to characterize the functional development of the enteric nervous system, the influence of gut microbiota on it, and based on the insights gained, proceed towards studying the same in disease models such as autism mutants. Based on recent studies mentioned earlier, our hypothesis is that we will likely observe a difference in the development of the ENS in germ-free larval zebrafish as compared to that of wild type. This will help understand the factors that microbiome shapes during development and the critical time-points of development, providing an optimal window for intervention. Along with this, in order to gain insight into the structural aspect of ENS development, we aim to carry out serial block face scanning electron microscopy (SBFSEM) analysis to investigate the dense meshwork of axons, dendrites and synapses that give rise to the enteric neuronal circuitry. This can further enable us to co-register the data from calcium imaging on to that from SBFSEM, allowing structure function comparison. This has been done in the past for the whole brain in larval zebrafish (Hildebrand et al., 2017).

1.2.3 Why zebrafish?

Zebrafish prove to be an ideal model for this study because the ENS in zebrafish larvae is conserved, in a simplified form, and is highly homologous to that in mammals (Wallace et al., 2005; Wang et al., 2010). This will enable us to extract important information that can be extended to other vertebrates. Zebrafish larvae are optically transparent, and this makes them a unique model that offers an unequalled opportunity for imaging activity in vivo. This allows us to establish causal links. The zebrafish gut is oriented straight along the rostro-caudal axis, which acts as an added advantage in terms of accessibility for imaging. This adds to the already existing array of excellent experimental attributes that this animal model provides, such as rapid development in an external environment, genetic tractability, large brood size and ease of housing (Grunwald et al., 2002).

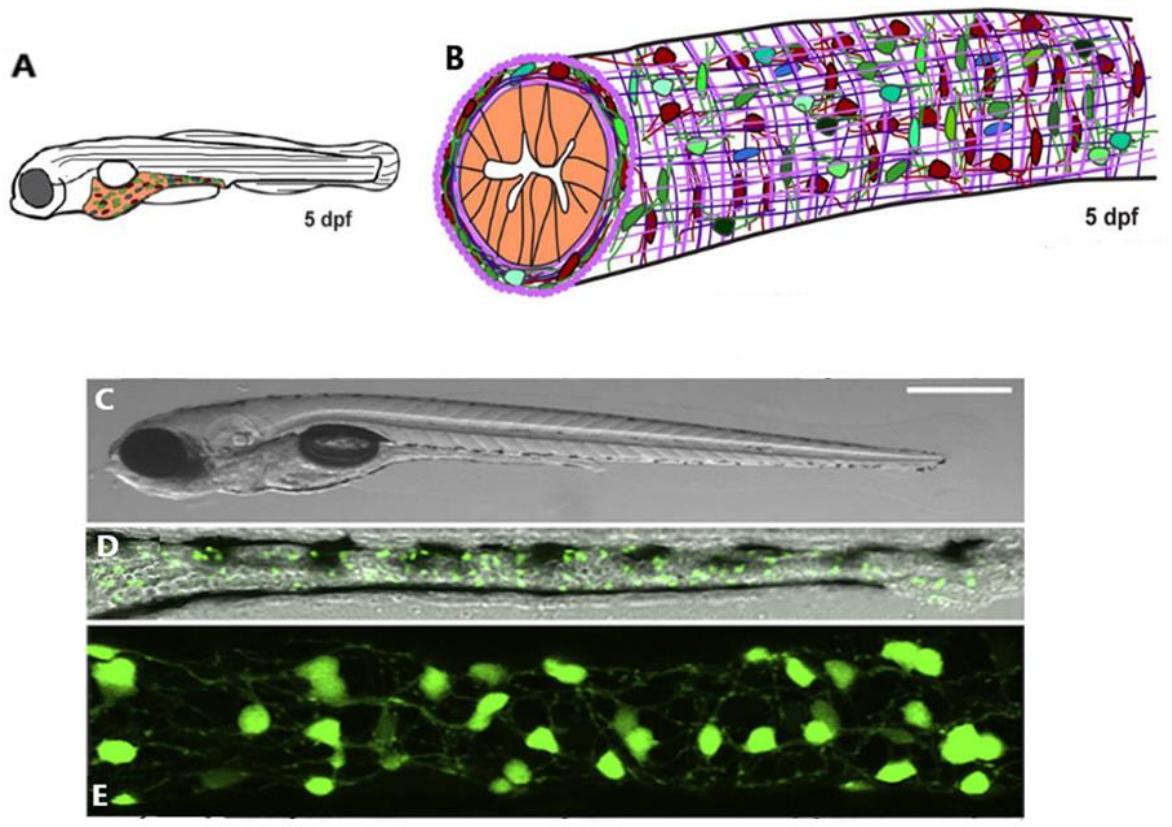

Figure 1.5: Zebrafish as a model for studying the function and development of the enteric nervous system. A) Overview of a 5 dpf larval zebrafish gut. B) Schematic showing a transverse section of a 5 dpf larval zebrafish gut. C) Side view of a 6 dpf zebrafish larva in bright field. D) Image of the posterior gut displaying enteric neurons labelled with *phox2b:GFP* (Taylor et al., 2016). E) High magnification image of the posterior gut. Scale bar= 500 µm (Adapted from: Ganz, J., 2018 and Kulkarni et al., 2018)

1.3 This project

In the project described in my thesis, I started out with the first part of the abovementioned plan, where I characterized the functional development of the ENS in wild-type zebrafish larvae. This stands out to be the first-ever study of its kind, with the aim to gain insight into how the enteric neural network forms, develops over time and brings about gut motility. I employed light-sheet microscopy to image the spontaneous activity of ENS neurons in 2 to 7 days post fertilization (dpf) zebrafish larvae using a nuclear-targeted genetically encoded calcium indicator, GCaMP6s (Chen et al., 2013). GCaMP6s is a calcium indicator that increases its intensity of fluorescence when it binds to calcium ions (Figure 1.6). It allows us to indirectly monitor the generation of action potentials in neurons by detecting the influx of calcium in neurons whenever they are active. A diffuse digitally scanned Selective Plane Illumination Microscope (SPIM) (Taylor et al., 2018) was used to obtain a volumetric movie of the activity across the ENS from GCaMP6s larvae. This methodology allowed to image spontaneous activity in the entire ENS. Further, I analysed the obtained datasets to gain an in-depth insight into the functional development and activity dynamics of the ENS over development.

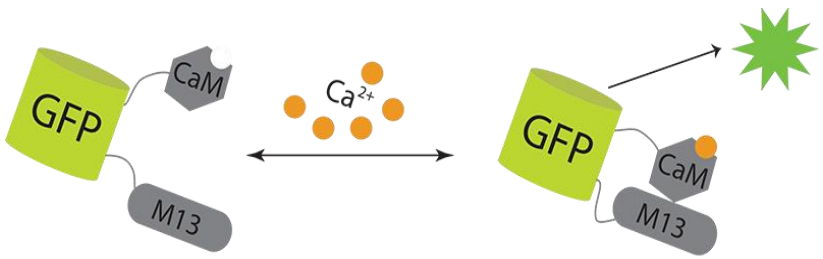

Figure 1.6: Mechanism of action of GCaMP. GCaMP biosensors are constructed by linking the N and C termini of GFP, creating new termini in the middle where calcium binding protein calmodulin (CaM) and its target peptide M13 are fused. When calcium is present within a cell, CaM binds to M13, causing a conformational change that increases the fluorescence. This provides us a proxy to detect neural activity. (Adapted from www.vigenebio.com)

Additionally, in order to gain insights into the anatomical arrangement of the dense ENS meshwork within the gut, we have carried out a trial run of serial block face scanning electron microscopy analysis in a 5 dpf zebrafish. I chose this age because it is known that most of the ENS is developed at 5 dpf. Older fish, for

example 7 dpf, are larger, which would lead to an enormous amount of data and issues of feasibility. Considering this and the physical limitations of fixation and sample treatments, 5 dpf seemed to be the best age to study allowing me to gather all the critical information, while reducing the amount of data I will have to process. This work will act as a first step towards the basic understanding of the functional development of the ENS in larval zebrafish. It will lay the groundwork for further investigation of the influence of gut microbiota on ENS development and future studies of the gut-brain axis in disease models.

Chapter 2
Materials and Methods

2.1 Animal models

All the work done with animals for this project was conducted in accordance with The University of Queensland Animal Welfare Unit (approved SBMS/378/16). Adult zebrafish were housed and maintained in a Techniplast zebrafish aquarium facility at 28.5 °C under standard conditions. For all the experiments, larvae carrying nuclear targeted *GCaMP6s* transgene under the pan-neuronal *HuC* promoter (*HuC:H2B-GCaMP6s*) (Chen et al., 2013) were used. Embryos were produced by natural breeding method and raised in petri dishes with embryo medium (1.37 mM NaCl, 53.65 µMKCl, 4.41 µM KH_2PO_4, 2.54 µM Na_2HPO_4, 0.13 mM $CaCl_2$, 0.16 mM $MgSO_4$, and 0.43 mM $NaHCO_3$ at pH ~7.2) and reared in an incubator 28.5 °C on a standard 14 hour on/ 10 hour off light cycle. At 2 or 3 dpf, once the larvae hatched out of their chorions, they were screened for GCaMP6s expression under a fluorescence microscope.

2.2 Sample preparation for calcium imaging

I imaged larvae embedded flat with their left side up in 2% low melting temperature agarose (Sigma A9045) and mounted on a custom-made 3D printed imaging chamber (Figure 2.1). Imaging chambers were made up of a 3D printed base (24 × 24 mm) with four posts (3 × 3 × 20 mm) at four of their corners and a glass coverslip (20 × 20 mm, 0.13-0.16 mm thick) fixed along the four vertical walls of the chambers.

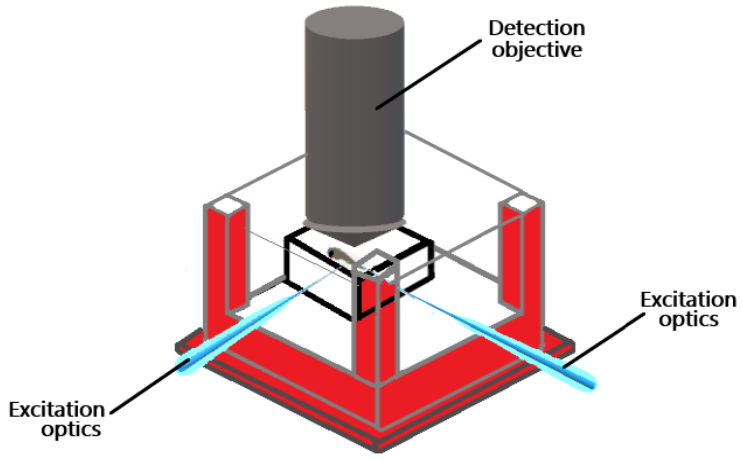

Figure 2.1: Schematic of the imaging setup. The immobilised larva is placed on a platform. The detection objective captures images from top while the excitation optics illuminate the sample perpendicularly along two sides.

Each chamber had a raised platform in its upper left quadrant (11 × 11 × 6 mm). Individual larvae were mounted onto these platforms and the chambers were filled with embryo medium after the agarose had set. I let the larvae settle for at least an hour before imaging.

2.3 Light sheet microscopy

Individual zebrafish larvae mounted on imaging chambers were imaged under a custom-built selective plane illumination microscope (Taylor et al., 2018) for their in vivo GCaMP6 activity within the gut. Two perpendicular laser planes were used for imaging (Figure 2.1). By employing this method, I could capture the spontaneous activity of the neurons in the ENS as well as the spinal cord at a time.

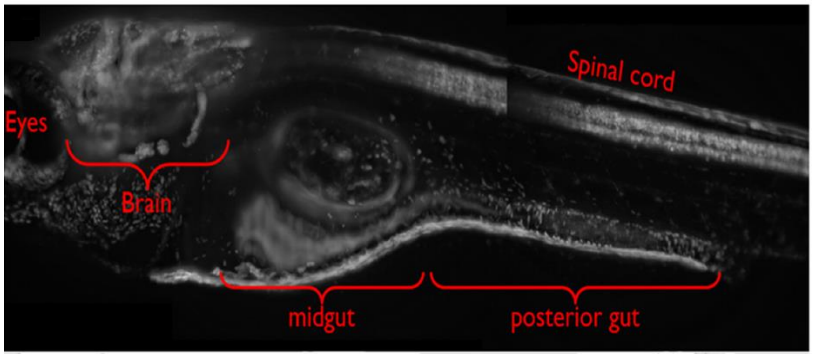

Figure 2.2: Tiled maximum intensity projection image of a 6 dpf larva expressing nuclear-targeted GCaMP6s transgene.

2.4 Recording parameters

All the recording parameters were managed remotely by a custom script using the micro-Manager software (Edelstein et al., 2010). The captured images were binned 4 times, resulting in a final resolution of 640 × 540 pixels at 16-bit in tagged image file (TIFF) format. For each larva, volumetric imaging was conducted wherein transverse planes spanning the entire volume of the ENS were imaged with 5 µm increments at 2 volumes per second for 10 minutes each in posterior- and the mid- gut. This resulted in a 16 to 20 GB movie comprising about 23 to 25 slices depending on the tilt during embedding the larva.

2.5 Pre-processing of the captured datasets

The volumetric calcium imaging data obtained was ultimately in the form of 4 dimensional stacks (x, y, z, time) which was converted to a concatenated time series for each transverse plane (23-25 planes per larva; x,y,time) using ImageJ v1.52c.

Then, a Non-Rigid Motion Correction (NoRMCorre) algorithm was used to correct for motion in the x-y plane (Pnevmatikakis and Giovannucci, 2017). Following this, an open source tool called CaImAn was used for segmentation (Giovannucci et al., 2019) http://github.com/flatironinstitute/CaImAn. CaImAn detects and extracts locations of individual neurons, referred to as regions of interest (ROIs) and at the same time demixes overlapping components (Figure 2.3). This prevents addition of the detected fluorescent signals providing a more accurate value of fluorescence changes for every ROI. For each ROI, individual fluorescent traces over time are extracted based on the dynamics of GCaMP6s (Figure 2.3 C).

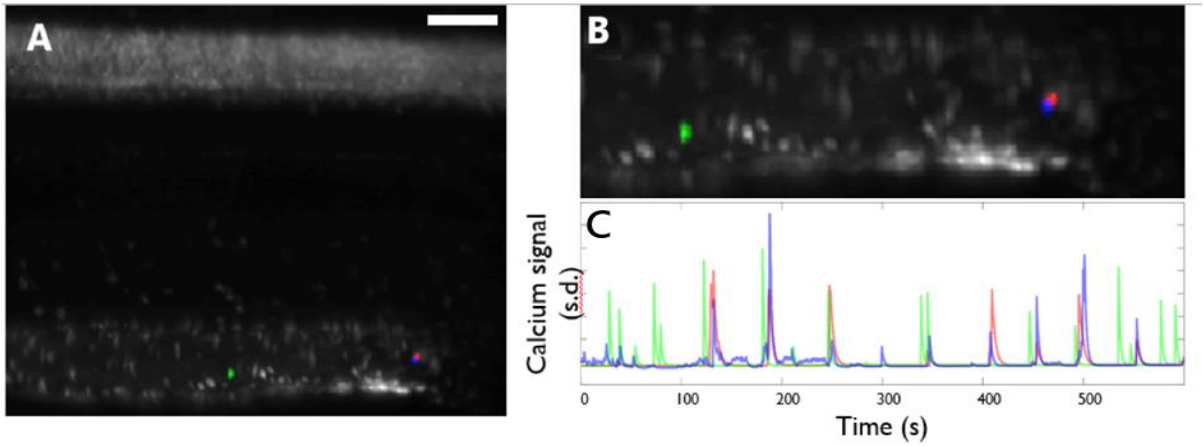

Figure 2.3: Image pre-processing. (A) An example demonstrating that three different neurons (represented in red, green and blue), including adjacent ones, can be detected by the CaImAn algorithm. Scale bar = 100μm. (B) Zoomed version of the neurons in A. (C) Z-scored de-noised calcium traces from the three neurons over time. The software could extract traces and de-mix neurons that are very closely located in space (red and blue).

2.6 Data analysis

The identified ROIs and their corresponding data were then pooled together and analysed using MATLAB R2018b (MathWorks). For t-SNE analysis, I used the MATLAB function tsne with correlation distance metric and the following parameters: Perplexity=50, Exaggeration=20. I used Ward's linkage for hierarchical clustering. For analysing the wave patterns, I used the sequential non-negative matrix factorization (seqNMF) toolbox (Mackevicius et al., 2019). The figures were produced using MATLAB R2018b and GraphPad Prism v8.0.1.

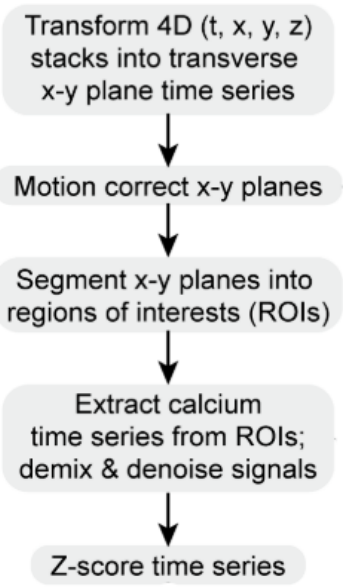

Figure 2.4: Bioinformatics pipeline for data pre-processing (Adapted from Constantin et al., 2019)

2.7 Statistical tests

All statistical tests were done using GraphPad Prism v8.0.1. For statistical comparison of number of ROIs over development, one-way ANOVA with tukey's multiple comparisons was employed. For testing the significance of probability distributions, two-way ANOVA with tukey's multiple comparisons was used.

2.8 Serial block face scanning electron microscopy (SBFSEM)

A 5 dpf larva was fixed in 2% formaldehyde and 2.5% glutaraldehyde fixative solution overnight at room temperature (Hildebrand et al., 2017). Following washes with PBS, the head and the tail of the larva was dissected off to keep only the middle portion of its body containing the intact gut. It was further processed by electron microscopy experts and subjected to SBFSEM with a nominal sectioning thickness of 50 nm and 4096 x 3530 voxels at 50nm resolution.

Chapter 3
Results

To investigate the ontogeny of the functional activity of the ENS, I performed volumetric calcium imaging of the ENS in 2 to 7 dpf larval zebrafish. I recorded the spontaneous activity of the ENS in the posterior gut and the mid-gut for a duration of 10 minutes each in each larva. Number of larvae imaged: 2 dpf (n=6), 3 dpf (n=9), 4 dpf (n=7), 5 dpf (n=7), 6 dpf (n=9), 7 dpf (n=7). The recorded data was in the form of four-dimensional stacks. I used ImageJ to convert it into one three-dimensional time series for each x-y plane. Following this, we sent the data to a high-performance computer for pre-processing. Pre-processing involved extracting information about the location of every neuron (ROI), motion correction, demixing and denoising. After pre-processing, I obtained outputs containing the ROIs' coordinates corresponding to individual neurons, and fluorescent traces across time for every ROI detected.

I analysed these identified ROIs and corresponding datasets using MATLAB to gain insights into how the ENS network develops over time. The ROIs detected included those found within the gut as well as the ones in the spinal cord. Therefore, I first separated them based on their x-y coordinates in space for each individual fish. I then correlated the calcium traces of the gut ROIs with that of a standard GCaMP6s signal, and only analysed the ones whose calcium traces showed a correlation above 0.6 and the ones that had more than three peaks of activity throughout the duration of the experiment.

3.1 Network growth over development

At 2 dpf, I observed no enteric innervation of the posterior gut while neurons from the spinal cord were observed. (Figure 3.1).

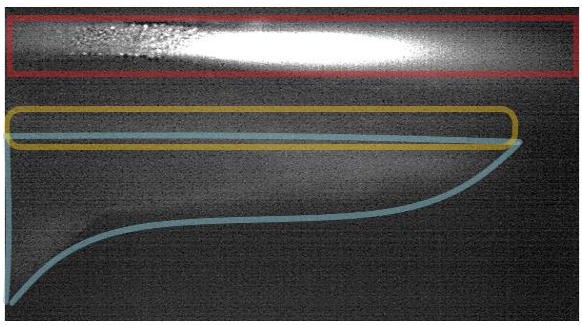

Figure 3.1: No neuronal innervation in 2 dpf larva. The area where the ENS expected is outlined yellow, yolk sac in blue and spinal cord in red. At 2 dpf, no ENS neurons were observed in the dataset.

To characterize the network growth dynamics over development, I plotted the number of gut neurons that were identified for each age (Figure 3.2). Overall, it was observed that the number of gut neurons increased from 3 dpf to 5 dpf and afterward decreased at 6 and 7 dpf. There is a significant increase in the number of ENS ROIs between 3 dpf and 5 dpf (p-value = 0.0005) as well as between 3dpf and 6 dpf (p-value = 0.0206). Also, a significant increase is observed in the number of ROIs between 4 and 5 dpf (p-value = 0.0378). This makes the 5 and 6 dpf significantly different from the rest of the age groups. It suggests that the network initially starts growing from 3 dpf, continues to grow until 5 dpf, and after that the number of ROIs declines back to similar to what was seen at 3 and 4 dpf.

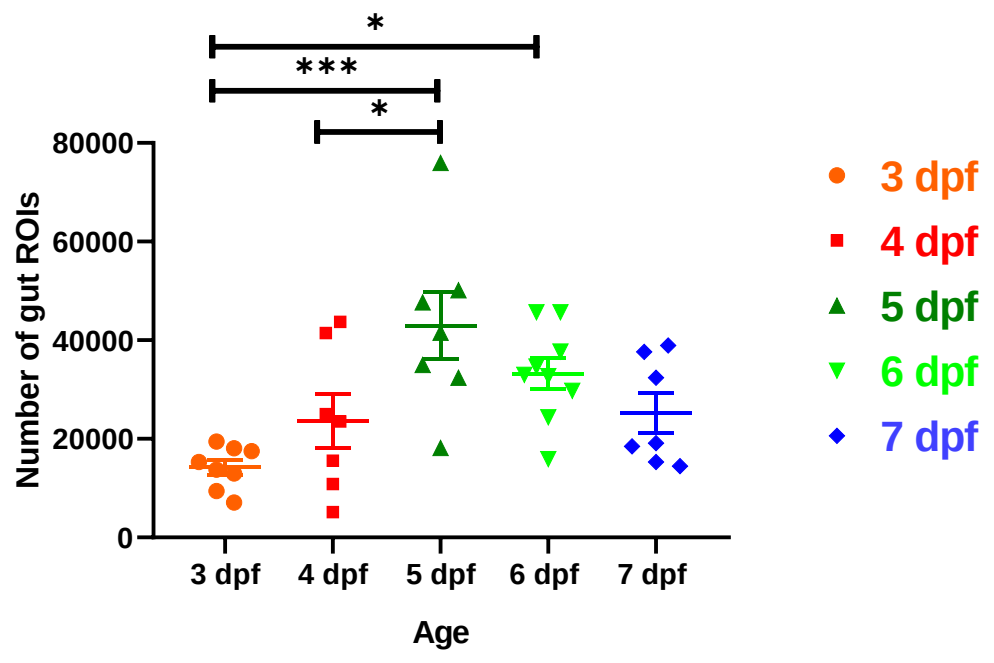

Figure 3.2: Network growth over development. The number of gut ROIs increases from 3 to 5 dpf and decreases later. Significant changes are observed in 3 versus 5 dpf (p-value = 0.0005), 3 versus 6 dpf (p-value = 0.0206) and 4 versus 5 dpf (p-value = 0.0378). Error bars represent means ± s.e.m.; each data point represents one individual larva, one-way ANOVA test with tukey's multiple comparisons, ****P*<0.001, **P*<0.05.

3.2 Network activity dynamics change over development

To investigate the statistics of spontaneous activity over development, I calculated the number of peaks or calcium events for every ROI detected. This was plotted for each age group, wherein each point on the y axis represents the probability that the observation shows those many number of peaks (x axis). The observations within each bin were normalized so that the sum of total probability is 1 for every age group (Figure 3.3).

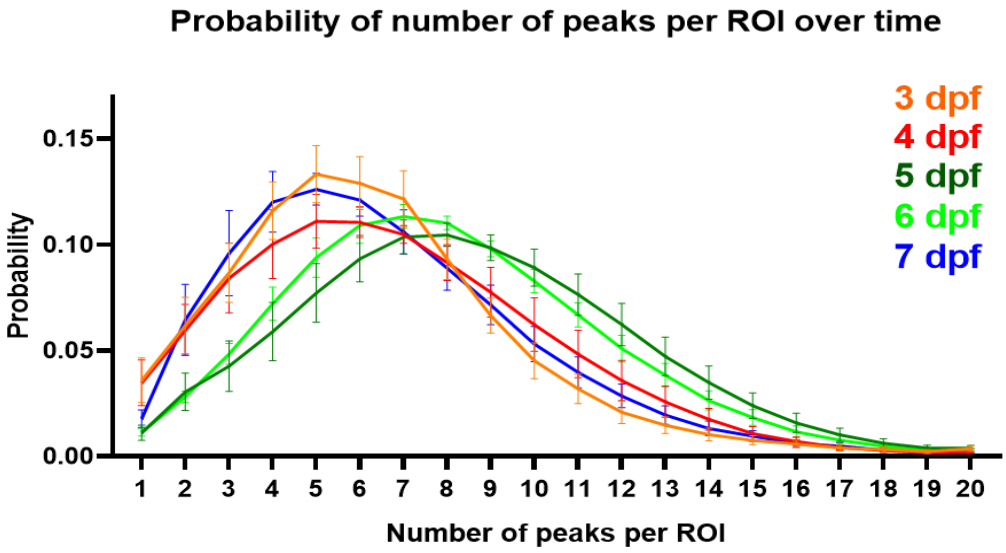

Figure 3.3: Network activity dynamics over development. The activity of ENS neurons increases from 3 dpf to 6 dpf and declines at 7 dpf. Error bars represent means ± s.e.m.; two-way ANOVA test with tukey's multiple comparisons, p-values listed in table 3.1.

I observed a higher probability of lower number of peaks per ROI around 3 to 4 dpf and it increases as the larvae grow, significantly from 5 to 6 dpf. However, we see that the activity reduces at 7 dpf. In order to test significance, I ran a two-way ANOVA with tukey's multiple comparisons test wherein I compared the probability for each value of number of peaks with its corresponding value in other age groups. The p-values for every comparison are listed in table 3.1. In summary, for lower number of peaks (2 to 5), there is a significant difference between 3-, 4-, 7- dpf and 5-, 6- dpf. There is a range (6 to 8 peaks) where there isn't a significant difference between 3-, 4-, 7- dpf and 5-, 6- dpf. Following this, for 9 to 12 peaks, there is a significant difference between 3 dpf and 5-, 6- dpf fishes. Based on this, it can be said that there is a trend where the activity of neurons increases from 3 dpf until around 6 dpf. However, further at 7 dpf the activity declines and becomes comparable to that observed at 3 and 4 dpf.

Table 3.1: List of p-values for tukey's multiple comparisons for number of peaks per ROI (N=peak number)

N=1	Significance	Adjusted p-values
3 dpf vs. 4 dpf	ns	>0.9999
3 dpf vs. 5 dpf	ns	0.1789
3 dpf vs. 6 dpf	ns	0.1345
3 dpf vs. 7 dpf	ns	0.4877
4 dpf vs. 5 dpf	ns	0.2777
4 dpf vs. 6 dpf	ns	0.2303
4 dpf vs. 7 dpf	ns	0.6134
5 dpf vs. 6 dpf	ns	>0.9999
5 dpf vs. 7 dpf	ns	0.9812
6 dpf vs. 7 dpf	ns	0.9793

N=2	Significance	Adjusted p-values
3 dpf vs. 4 dpf	ns	0.9997
3 dpf vs. 5 dpf	*	0.0433
3 dpf vs. 6 dpf	*	0.0126
3 dpf vs. 7 dpf	ns	0.9993
4 dpf vs. 5 dpf	ns	0.1037
4 dpf vs. 6 dpf	*	0.0417
4 dpf vs. 7 dpf	ns	0.9943
5 dpf vs. 6 dpf	ns	0.9996
5 dpf vs. 7 dpf	*	0.0358
6 dpf vs. 7 dpf	*	0.0113

N=3	Significance	Adjusted p-values
3 dpf vs. 4 dpf	ns	0.9995
3 dpf vs. 5 dpf	***	0.0009
3 dpf vs. 6 dpf	**	0.0026
3 dpf vs. 7 dpf	ns	0.9226
4 dpf vs. 5 dpf	**	0.0046
4 dpf vs. 6 dpf	*	0.0127
4 dpf vs. 7 dpf	ns	0.8628
5 dpf vs. 6 dpf	ns	0.9861
5 dpf vs. 7 dpf	****	<0.0001
6 dpf vs. 7 dpf	***	0.0002

N=4	Significance	Adjusted p-values
3 dpf vs. 4 dpf	ns	0.6231
3 dpf vs. 5 dpf	****	<0.0001
3 dpf vs. 6 dpf	***	0.0003
3 dpf vs. 7 dpf	ns	0.9962
4 dpf vs. 5 dpf	**	0.0051
4 dpf vs. 6 dpf	ns	0.0906
4 dpf vs. 7 dpf	ns	0.4519
5 dpf vs. 6 dpf	ns	0.7695
5 dpf vs. 7 dpf	****	<0.0001
6 dpf vs. 7 dpf	***	0.0002

N=5	Significance	Adjusted p-values
3 dpf vs. 4 dpf	ns	0.2769
3 dpf vs. 5 dpf	****	<0.0001
3 dpf vs. 6 dpf	**	0.0018
3 dpf vs. 7 dpf	ns	0.9703
4 dpf vs. 5 dpf	*	0.0378
4 dpf vs. 6 dpf	ns	0.5472
4 dpf vs. 7 dpf	ns	0.7078
5 dpf vs. 6 dpf	ns	0.5735
5 dpf vs. 7 dpf	***	0.0004
6 dpf vs. 7 dpf	*	0.0338

N=6	Significance	Adjusted p-values
3 dpf vs. 4 dpf	ns	0.4713
3 dpf vs. 5 dpf	*	0.0135
3 dpf vs. 6 dpf	ns	0.3218
3 dpf vs. 7 dpf	ns	0.9556
4 dpf vs. 5 dpf	ns	0.5979
4 dpf vs. 6 dpf	ns	>0.9999
4 dpf vs. 7 dpf	ns	0.9028
5 dpf vs. 6 dpf	ns	0.6251
5 dpf vs. 7 dpf	ns	0.1366
6 dpf vs. 7 dpf	ns	0.8233

N=7	Significance	Adjusted p-values
3 dpf vs. 4 dpf	ns	0.571
3 dpf vs. 5 dpf	ns	0.5029
3 dpf vs. 6 dpf	ns	0.9367
3 dpf vs. 7 dpf	ns	0.6426
4 dpf vs. 5 dpf	ns	>0.9999
4 dpf vs. 6 dpf	ns	0.9421
4 dpf vs. 7 dpf	ns	>0.9999
5 dpf vs. 6 dpf	ns	0.91
5 dpf vs. 7 dpf	ns	0.9996
6 dpf vs. 7 dpf	ns	0.9669

N=8	Significance	Adjusted p-values
3 dpf vs. 4 dpf	ns	>0.9999
3 dpf vs. 5 dpf	ns	0.8414
3 dpf vs. 6 dpf	ns	0.4743
3 dpf vs. 7 dpf	ns	0.9959
4 dpf vs. 5 dpf	ns	0.807
4 dpf vs. 6 dpf	ns	0.4554
4 dpf vs. 7 dpf	ns	0.9994
5 dpf vs. 6 dpf	ns	0.9873
5 dpf vs. 7 dpf	ns	0.6769
6 dpf vs. 7 dpf	ns	0.316

N=9	Significance	Adjusted p-values
3 dpf vs. 4 dpf	ns	0.8664
3 dpf vs. 5 dpf	*	0.0368
3 dpf vs. 6 dpf	*	0.0235
3 dpf vs. 7 dpf	ns	0.992
4 dpf vs. 5 dpf	ns	0.3962
4 dpf vs. 6 dpf	ns	0.3575
4 dpf vs. 7 dpf	ns	0.9872
5 dpf vs. 6 dpf	ns	>0.9999
5 dpf vs. 7 dpf	ns	0.1579
6 dpf vs. 7 dpf	ns	0.1274

N=10	Significance	Adjusted p-values
3 dpf vs. 4 dpf	ns	0.5505
3 dpf vs. 5 dpf	***	0.0009
3 dpf vs. 6 dpf	**	0.0033
3 dpf vs. 7 dpf	ns	0.9555
4 dpf vs. 5 dpf	ns	0.1596
4 dpf vs. 6 dpf	ns	0.3541
4 dpf vs. 7 dpf	ns	0.9397
5 dpf vs. 6 dpf	ns	0.9805
5 dpf vs. 7 dpf	*	0.0215
6 dpf vs. 7 dpf	ns	0.0628

Table 3.1 (continued): List of p-values for tukey's multiple comparisons for number of peaks per ROI (N=peak number)

N=11	Significance	Adjusted p-values
3 dpf vs. 4 dpf	ns	0.5882
3 dpf vs. 5 dpf	***	0.0008
3 dpf vs. 6 dpf	**	0.0084
3 dpf vs. 7 dpf	ns	0.9587
4 dpf vs. 5 dpf	ns	0.129
4 dpf vs. 6 dpf	ns	0.4699
4 dpf vs. 7 dpf	ns	0.9501
5 dpf vs. 6 dpf	ns	0.9131
5 dpf vs. 7 dpf	*	0.0181
6 dpf vs. 7 dpf	ns	0.1124

N=12	Significance	Adjusted p-values
3 dpf vs. 4 dpf	ns	0.6693
3 dpf vs. 5 dpf	**	0.0023
3 dpf vs. 6 dpf	*	0.0355
3 dpf vs. 7 dpf	ns	0.9592
4 dpf vs. 5 dpf	ns	0.1742
4 dpf vs. 6 dpf	ns	0.6677
4 dpf vs. 7 dpf	ns	0.9734
5 dpf vs. 6 dpf	ns	0.8485
5 dpf vs. 7 dpf	*	0.0386
6 dpf vs. 7 dpf	ns	0.2743

N=13	Significance	Adjusted p-values
3 dpf vs. 4 dpf	ns	0.8609
3 dpf vs. 5 dpf	*	0.0321
3 dpf vs. 6 dpf	ns	0.1622
3 dpf vs. 7 dpf	ns	0.9931
4 dpf vs. 5 dpf	ns	0.3764
4 dpf vs. 6 dpf	ns	0.7967
4 dpf vs. 7 dpf	ns	0.9843
5 dpf vs. 6 dpf	ns	0.9344
5 dpf vs. 7 dpf	ns	0.1379
6 dpf vs. 7 dpf	ns	0.4468

N=14	Significance	Adjusted p-values
3 dpf vs. 4 dpf	ns	0.9676
3 dpf vs. 5 dpf	ns	0.1867
3 dpf vs. 6 dpf	ns	0.5423
3 dpf vs. 7 dpf	ns	0.9991
4 dpf vs. 5 dpf	ns	0.5943
4 dpf vs. 6 dpf	ns	0.9342
4 dpf vs. 7 dpf	ns	0.9961
5 dpf vs. 6 dpf	ns	0.9439
5 dpf vs. 7 dpf	ns	0.3624
6 dpf vs. 7 dpf	ns	0.7634

N=15	Significance	Adjusted p-values
3 dpf vs. 4 dpf	ns	0.9987
3 dpf vs. 5 dpf	ns	0.5927
3 dpf vs. 6 dpf	ns	0.8466
3 dpf vs. 7 dpf	ns	0.9998
4 dpf vs. 5 dpf	ns	0.8027
4 dpf vs. 6 dpf	ns	0.9621
4 dpf vs. 7 dpf	ns	>0.9999
5 dpf vs. 6 dpf	ns	0.9873
5 dpf vs. 7 dpf	ns	0.7491
6 dpf vs. 7 dpf	ns	0.9375

N=16	Significance	Adjusted p-values
3 dpf vs. 4 dpf	ns	>0.9999
3 dpf vs. 5 dpf	ns	0.9024
3 dpf vs. 6 dpf	ns	0.9818
3 dpf vs. 7 dpf	ns	>0.9999
4 dpf vs. 5 dpf	ns	0.9493
4 dpf vs. 6 dpf	ns	0.9943
4 dpf vs. 7 dpf	ns	>0.9999
5 dpf vs. 6 dpf	ns	0.996
5 dpf vs. 7 dpf	ns	0.9244
6 dpf vs. 7 dpf	ns	0.9873

N=17	Significance	Adjusted p-values
3 dpf vs. 4 dpf	ns	>0.9999
3 dpf vs. 5 dpf	ns	0.981
3 dpf vs. 6 dpf	ns	0.9964
3 dpf vs. 7 dpf	ns	>0.9999
4 dpf vs. 5 dpf	ns	0.9872
4 dpf vs. 6 dpf	ns	0.998
4 dpf vs. 7 dpf	ns	>0.9999
5 dpf vs. 6 dpf	ns	0.9995
5 dpf vs. 7 dpf	ns	0.9921
6 dpf vs. 7 dpf	ns	0.9992

N=18	Significance	Adjusted p-values
3 dpf vs. 4 dpf	ns	>0.9999
3 dpf vs. 5 dpf	ns	0.9987
3 dpf vs. 6 dpf	ns	0.9999
3 dpf vs. 7 dpf	ns	>0.9999
4 dpf vs. 5 dpf	ns	0.9982
4 dpf vs. 6 dpf	ns	0.9997
4 dpf vs. 7 dpf	ns	>0.9999
5 dpf vs. 6 dpf	ns	>0.9999
5 dpf vs. 7 dpf	ns	0.9988
6 dpf vs. 7 dpf	ns	0.9999

N=19	Significance	Adjusted p-values
3 dpf vs. 4 dpf	ns	>0.9999
3 dpf vs. 5 dpf	ns	0.9999
3 dpf vs. 6 dpf	ns	>0.9999
3 dpf vs. 7 dpf	ns	>0.9999
4 dpf vs. 5 dpf	ns	0.9997
4 dpf vs. 6 dpf	ns	>0.9999
4 dpf vs. 7 dpf	ns	>0.9999
5 dpf vs. 6 dpf	ns	>0.9999
5 dpf vs. 7 dpf	ns	0.9999
6 dpf vs. 7 dpf	ns	>0.9999

N=20	Significance	Adjusted p-values
3 dpf vs. 4 dpf	ns	0.9998
3 dpf vs. 5 dpf	ns	>0.9999
3 dpf vs. 6 dpf	ns	>0.9999
3 dpf vs. 7 dpf	ns	>0.9999
4 dpf vs. 5 dpf	ns	0.9998
4 dpf vs. 6 dpf	ns	>0.9999
4 dpf vs. 7 dpf	ns	>0.9999
5 dpf vs. 6 dpf	ns	>0.9999
5 dpf vs. 7 dpf	ns	>0.9999
6 dpf vs. 7 dpf	ns	>0.9999

3.3. Characteristics of the waves of peristalsis that are observed

The dynamics of activity differed over different developmental time-points from 3 to 7 dpf. At 3 dpf, I observed less neurons that fired randomly whereas at 6dpf, a lot more neurons participated in the activity and the pattern seemed to be more organised, exhibiting waves (Figure 3.4). These waves correspond to the peristaltic activity brought about by the ENS (Figure 3.5).

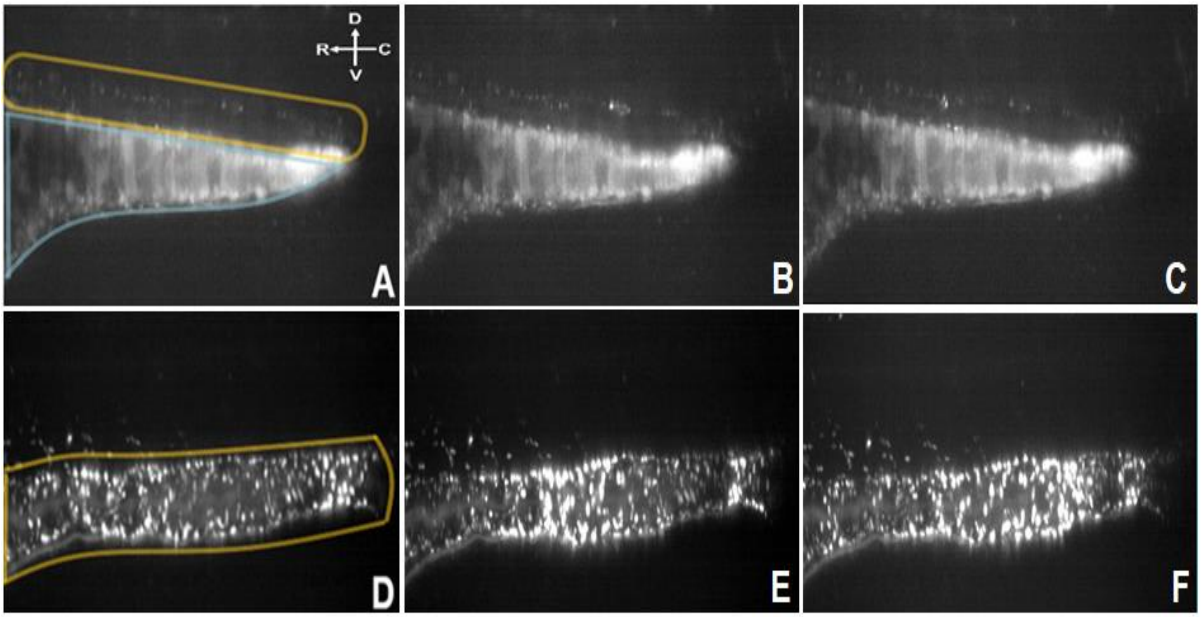

Figure 3.4: Activity pattern over development. The posterior gut is outlined in yellow and the yolk sac in blue. Body axis orientations are shown in panel A on top right. R=Rostral, C=Caudal, D=Dorsal, V=Ventral. (A-C) Snapshots of activity within a 3 dpf old fish. The small spots are neurons. (D-F) Snapshots of activity within a 6 dpf old larva. Between 3 and 6 dpf, the activity changes from very low to high. D-F shows a wave observed in a 6 dpf larva.

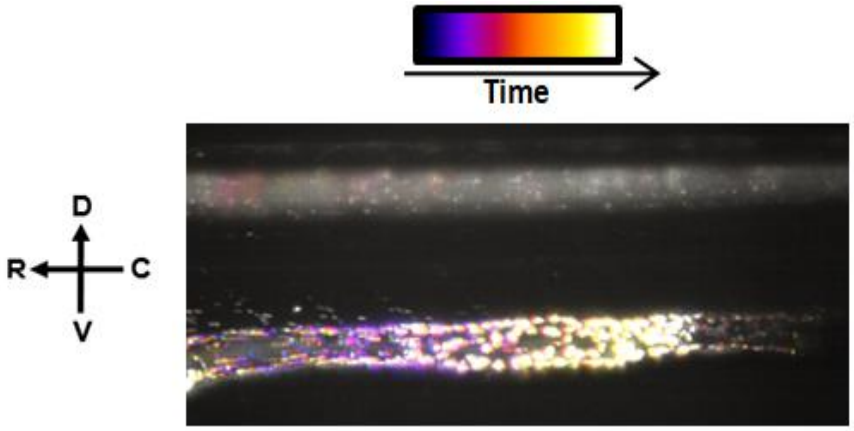

Figure 3.5: Waves of peristalsis: A wave from 6 dpf larva, colour coded temporally with earlier events in purple and later events in white.

3.3.1 Correlated activity changes over development

In order to characterize these patterns of activity, I computed the correlation distance between all ROIs for each fish and plotted the probability distribution for correlation at each age group (Figure 3.6). The observations within each bin were normalized so that the sum of total probability is 1 for every age group. There seems to be a positive correlation bias at younger ages (3- and 4- dpf) which reduces in older fish from 5 dpf. At 7 dpf, a negative correlation (or anti-correlation) is observed. To test the significance, I ran a two-way ANOVA with tukey's multiple comparisons test where I compared the probability for each correlation value with its corresponding value in other age groups. The p-values are listed in table 3.2. Based on these, a significant difference was observed in the positively correlated activity seen in 3 versus 5 dpf, 3 versus 6 dpf, 3 versus 7 dpf. However, no significant difference was observed with respect to the anti-correlated activity. The 4 dpf stage might be displaying a transition from more correlated to less correlated. In summary, there was a significant difference in the correlated activity observed between 3 dpf and 5, 6, 7 dpf and a trend where the neurons tend to be anti-correlated at 7 dpf.

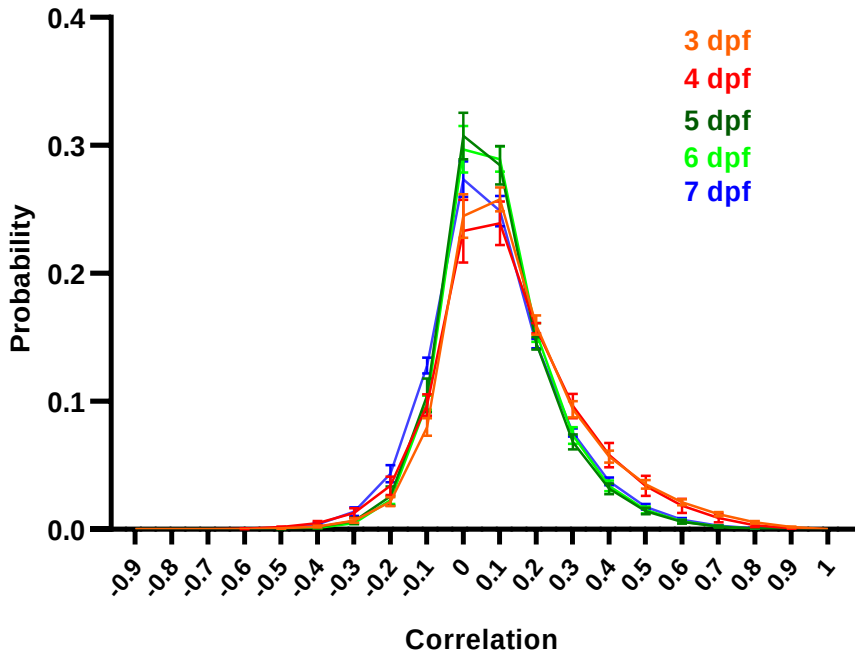

Figure 3.6: Correlation present early during development that declines from 5dpf. Positive correlation is seen at younger ages (3 and 4 dpf), which reduces from 5 dpf. Error bars represent means ± s.e.m.; two-way ANOVA test with tukey's multiple comparisons, p-values listed in table 3.2.

Table 3.2: List of p-values for tukey's multiple comparisons for correlation across age

Correlation=0.9	Significance	Adjusted p-values
3 dpf vs. 4 dpf	ns	0.5155
3 dpf vs. 5 dpf	*	0.019
3 dpf vs. 6 dpf	*	0.0182
3 dpf vs. 7 dpf	*	0.0217
4 dpf vs. 5 dpf	ns	0.5227
4 dpf vs. 6 dpf	ns	0.5066
4 dpf vs. 7 dpf	ns	0.5713
5 dpf vs. 6 dpf	ns	0.9994
5 dpf vs. 7 dpf	ns	0.9802
6 dpf vs. 7 dpf	ns	0.9392

Correlation=1	Significance	Adjusted p-values
3 dpf vs. 4 dpf	ns	0.7357
3 dpf vs. 5 dpf	*	0.0284
3 dpf vs. 6 dpf	*	0.0191
3 dpf vs. 7 dpf	*	0.0345
4 dpf vs. 5 dpf	ns	0.662
4 dpf vs. 6 dpf	ns	0.5282
4 dpf vs. 7 dpf	ns	0.7113
5 dpf vs. 6 dpf	ns	0.9094
5 dpf vs. 7 dpf	ns	0.9956
6 dpf vs. 7 dpf	ns	0.4631

Correlation=0.8	Significance	Adjusted p-values
3 dpf vs. 4 dpf	ns	0.7385
3 dpf vs. 5 dpf	**	0.0062
3 dpf vs. 6 dpf	**	0.0063
3 dpf vs. 7 dpf	**	0.0076
4 dpf vs. 5 dpf	ns	0.4567
4 dpf vs. 6 dpf	ns	0.4662
4 dpf vs. 7 dpf	ns	0.5078
5 dpf vs. 6 dpf	ns	>0.9999
5 dpf vs. 7 dpf	ns	0.9739
6 dpf vs. 7 dpf	ns	0.9895

Correlation=0.7	Significance	Adjusted p-values
3 dpf vs. 4 dpf	ns	0.9197
3 dpf vs. 5 dpf	**	0.0016
3 dpf vs. 6 dpf	**	0.0017
3 dpf vs. 7 dpf	**	0.0025
4 dpf vs. 5 dpf	ns	0.3684
4 dpf vs. 6 dpf	ns	0.3855
4 dpf vs. 7 dpf	ns	0.4414
5 dpf vs. 6 dpf	ns	0.9998
5 dpf vs. 7 dpf	ns	0.9412
6 dpf vs. 7 dpf	ns	0.9794

Correlation=0.6	Significance	Adjusted p-values
3 dpf vs. 4 dpf	ns	0.9897
3 dpf vs. 5 dpf	***	0.0007
3 dpf vs. 6 dpf	***	0.0008
3 dpf vs. 7 dpf	**	0.0017
4 dpf vs. 5 dpf	ns	0.288
4 dpf vs. 6 dpf	ns	0.3112
4 dpf vs. 7 dpf	ns	0.3913
5 dpf vs. 6 dpf	ns	0.9996
5 dpf vs. 7 dpf	ns	0.8912
6 dpf vs. 7 dpf	ns	0.957

Correlation=0.5	Significance	Adjusted p-values
3 dpf vs. 4 dpf	ns	0.9999
3 dpf vs. 5 dpf	**	0.0017
3 dpf vs. 6 dpf	**	0.002
3 dpf vs. 7 dpf	**	0.0052
4 dpf vs. 5 dpf	ns	0.2236
4 dpf vs. 6 dpf	ns	0.2559
4 dpf vs. 7 dpf	ns	0.3579
5 dpf vs. 6 dpf	ns	0.9989
5 dpf vs. 7 dpf	ns	0.841
6 dpf vs. 7 dpf	ns	0.9403

Correlation=0.2	Significance	Adjusted p-values
3 dpf vs. 4 dpf	ns	0.9979
3 dpf vs. 5 dpf	ns	0.5324
3 dpf vs. 6 dpf	ns	0.9812
3 dpf vs. 7 dpf	ns	0.4633
4 dpf vs. 5 dpf	ns	0.3855
4 dpf vs. 6 dpf	ns	0.9951
4 dpf vs. 7 dpf	ns	0.2467
5 dpf vs. 6 dpf	ns	0.8634
5 dpf vs. 7 dpf	ns	>0.9999
6 dpf vs. 7 dpf	ns	0.8194

Correlation=0.1	Significance	Adjusted p-values
3 dpf vs. 4 dpf	ns	0.8664
3 dpf vs. 5 dpf	ns	0.5783
3 dpf vs. 6 dpf	ns	0.1914
3 dpf vs. 7 dpf	ns	0.9725
4 dpf vs. 5 dpf	ns	0.3202
4 dpf vs. 6 dpf	ns	0.153
4 dpf vs. 7 dpf	ns	0.9892
5 dpf vs. 6 dpf	ns	0.9987
5 dpf vs. 7 dpf	ns	0.3804
6 dpf vs. 7 dpf	ns	0.1201

Correlation=0.4	Significance	Adjusted p-values
3 dpf vs. 4 dpf	ns	>0.9999
3 dpf vs. 5 dpf	**	0.0097
3 dpf vs. 6 dpf	*	0.0164
3 dpf vs. 7 dpf	*	0.0269
4 dpf vs. 5 dpf	ns	0.177
4 dpf vs. 6 dpf	ns	0.2354
4 dpf vs. 7 dpf	ns	0.337
5 dpf vs. 6 dpf	ns	0.9954
5 dpf vs. 7 dpf	ns	0.7969
6 dpf vs. 7 dpf	ns	0.9572

Correlation=0.3	Significance	Adjusted p-values
3 dpf vs. 4 dpf	ns	0.9995
3 dpf vs. 5 dpf	ns	0.064
3 dpf vs. 6 dpf	ns	0.212
3 dpf vs. 7 dpf	ns	0.1367
4 dpf vs. 5 dpf	ns	0.16
4 dpf vs. 6 dpf	ns	0.3278
4 dpf vs. 7 dpf	ns	0.3194
5 dpf vs. 6 dpf	ns	0.9764
5 dpf vs. 7 dpf	ns	0.7987
6 dpf vs. 7 dpf	ns	0.9977

Table 3.2 (continued): List of p-values for tukey's multiple comparisons for correlation across age.

Correlation=0	Significance	Adjusted p-values
3 dpf vs. 4 dpf	ns	0.9941
3 dpf vs. 5 dpf	ns	0.1448
3 dpf vs. 6 dpf	ns	0.2664
3 dpf vs. 7 dpf	ns	0.6859
4 dpf vs. 5 dpf	ns	0.178
4 dpf vs. 6 dpf	ns	0.2859
4 dpf vs. 7 dpf	ns	0.6211
5 dpf vs. 6 dpf	ns	0.9935
5 dpf vs. 7 dpf	ns	0.6001
6 dpf vs. 7 dpf	ns	0.8436

Correlation= -0.7	Significance	Adjusted p-values
3 dpf vs. 4 dpf	ns	0.7363
3 dpf vs. 5 dpf	ns	0.5345
3 dpf vs. 6 dpf	ns	0.1966
3 dpf vs. 7 dpf	ns	0.9137
4 dpf vs. 5 dpf	ns	0.4529
4 dpf vs. 6 dpf	ns	0.3722
4 dpf vs. 7 dpf	ns	0.5695
5 dpf vs. 6 dpf	ns	0.8699
5 dpf vs. 7 dpf	ns	0.924
6 dpf vs. 7 dpf	ns	0.4542

Correlation= -0.6	Significance	Adjusted p-values
3 dpf vs. 4 dpf	ns	0.6585
3 dpf vs. 5 dpf	ns	0.8168
3 dpf vs. 6 dpf	ns	0.2622
3 dpf vs. 7 dpf	ns	>0.9999
4 dpf vs. 5 dpf	ns	0.4185
4 dpf vs. 6 dpf	ns	0.2952
4 dpf vs. 7 dpf	ns	0.6538
5 dpf vs. 6 dpf	ns	0.8766
5 dpf vs. 7 dpf	ns	0.8951
6 dpf vs. 7 dpf	ns	0.4611

Correlation= -0.5	Significance	Adjusted p-values
3 dpf vs. 4 dpf	ns	0.5808
3 dpf vs. 5 dpf	ns	0.9543
3 dpf vs. 6 dpf	ns	0.341
3 dpf vs. 7 dpf	ns	0.9759
4 dpf vs. 5 dpf	ns	0.394
4 dpf vs. 6 dpf	ns	0.2147
4 dpf vs. 7 dpf	ns	0.8485
5 dpf vs. 6 dpf	ns	0.8811
5 dpf vs. 7 dpf	ns	0.8046
6 dpf vs. 7 dpf	ns	0.3795

Correlation= -0.4	Significance	Adjusted p-values
3 dpf vs. 4 dpf	ns	0.6107
3 dpf vs. 5 dpf	ns	0.9927
3 dpf vs. 6 dpf	ns	0.5188
3 dpf vs. 7 dpf	ns	0.7567
4 dpf vs. 5 dpf	ns	0.4995
4 dpf vs. 6 dpf	ns	0.2556
4 dpf vs. 7 dpf	ns	0.9938
5 dpf vs. 6 dpf	ns	0.9158
5 dpf vs. 7 dpf	ns	0.6243
6 dpf vs. 7 dpf	ns	0.271

Correlation= -0.3	Significance	Adjusted p-values
3 dpf vs. 4 dpf	ns	0.6147
3 dpf vs. 5 dpf	ns	>0.9999
3 dpf vs. 6 dpf	ns	0.8823
3 dpf vs. 7 dpf	ns	0.3863
4 dpf vs. 5 dpf	ns	0.6783
4 dpf vs. 6 dpf	ns	0.3612
4 dpf vs. 7 dpf	ns	0.9997
5 dpf vs. 6 dpf	ns	0.9694
5 dpf vs. 7 dpf	ns	0.4774
6 dpf vs. 7 dpf	ns	0.1817

Correlation= -0.2	Significance	Adjusted p-values
3 dpf vs. 4 dpf	ns	0.5517
3 dpf vs. 5 dpf	ns	0.9817
3 dpf vs. 6 dpf	ns	0.9989
3 dpf vs. 7 dpf	ns	0.0901
4 dpf vs. 5 dpf	ns	0.9303
4 dpf vs. 6 dpf	ns	0.6175
4 dpf vs. 7 dpf	ns	0.8629
5 dpf vs. 6 dpf	ns	0.9939
5 dpf vs. 7 dpf	ns	0.4351
6 dpf vs. 7 dpf	ns	0.108

Correlation= -0.1	Significance	Adjusted p-values
3 dpf vs. 4 dpf	ns	0.5303
3 dpf vs. 5 dpf	ns	0.4911
3 dpf vs. 6 dpf	ns	0.2419
3 dpf vs. 7 dpf	***	0.001
4 dpf vs. 5 dpf	ns	0.9864
4 dpf vs. 6 dpf	ns	0.9997
4 dpf vs. 7 dpf	ns	0.0725
5 dpf vs. 6 dpf	ns	0.9932
5 dpf vs. 7 dpf	ns	0.5234
6 dpf vs. 7 dpf	*	0.0237

3.3.2 The ENS circuit evolves over development

To delve deeper into understanding the circuit development, I plotted the ROIs in 2D, clustered them and ultimately mapped these clusters of ROIs spatially according to their coordinates within the gut. This allowed us to visualise clusters of correlated ROIs within the gut over development. I employed t-distributed Stochastic Neighbour Embedding (t-SNE), a dimensionality reduction tool that is useful for visualizing high dimensional datasets, to plot the ROIs in 2D. I used the MATLAB function tsne to embed the ROIs from the 4 dimensional dataset (x,y,z,t) in 2 dimensions using correlation as a distance. Once the ROIs were plotted in 2D, I used Ward's linkage for hierarchical clustering and plotted the identified clusters in 2D (Figure 3.7).

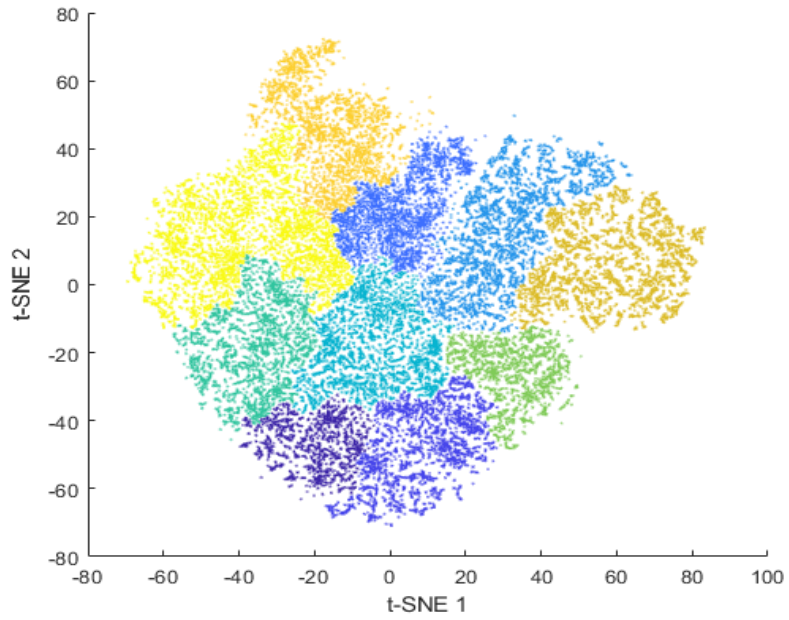

Figure 3.7: Segregated ROI clusters for a 3 dpf larva in 2 dimensions. The ROIs belonging to functional clusters are represented in 2D following a t-SNE analysis.

I further mapped these ROIs onto the gut using their coordinates with different colours representing the clusters that they belonged to (Figure 3.8). At 3 dpf, there are smaller clusters of ROIs that span a smaller area within the gut, and fire together. At 4 dpf a similar trend is seen with slight mixing of clusters towards the rostral and middle part of the gut. From 5 dpf onwards, the clusters start intermingling and mixing. This represents the large coordinated waves that start arising from this age. By 7 dpf, these waves of peristalsis seem to be fully developed

and span much larger lengths of the gut. One point to notice is the smaller clusters observed towards the caudal end of the gut that persist even at 6 and 7 dpf.

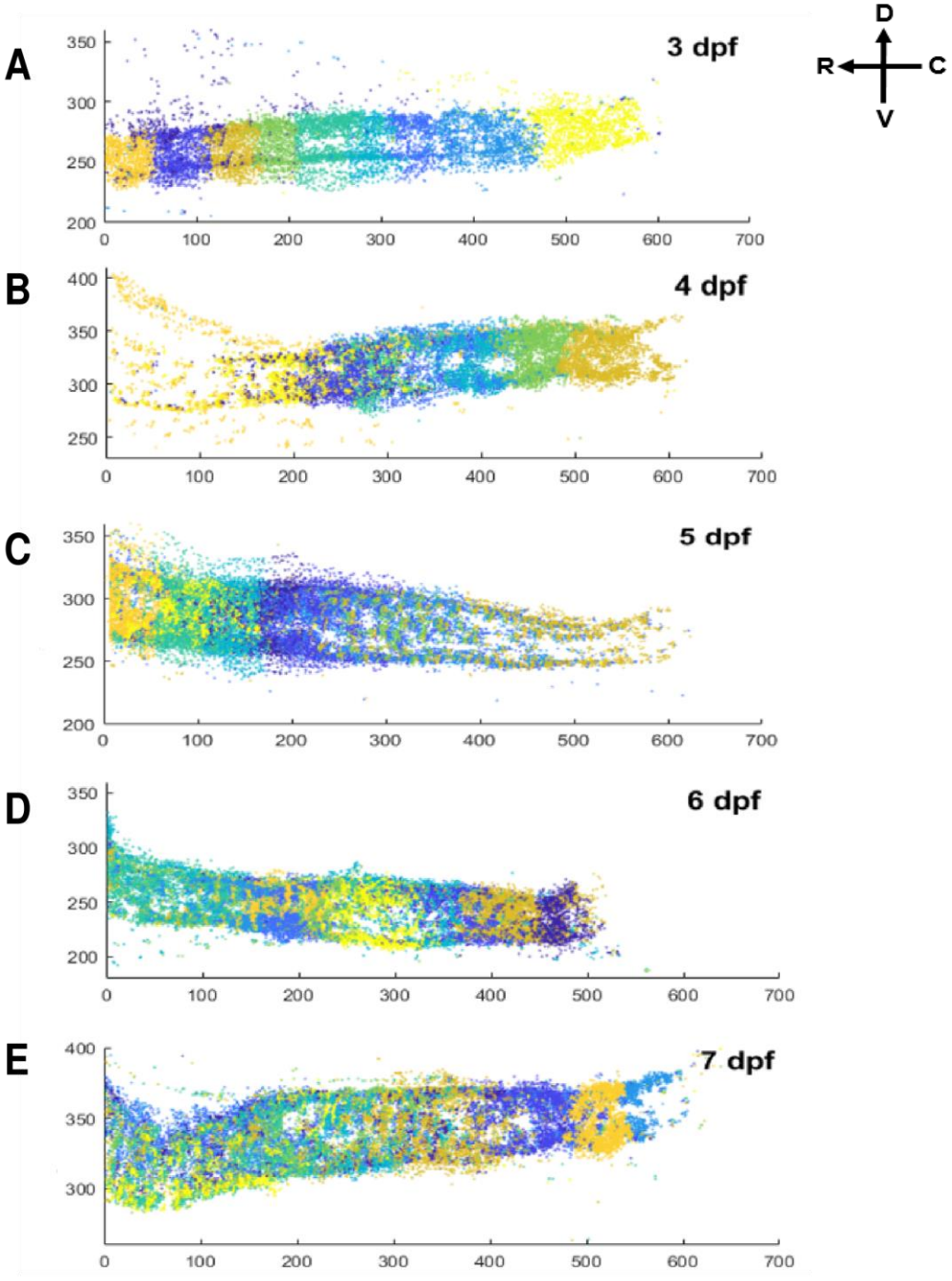

Figure 3.8: ENS circuitry evolves over development. The gut ROIs are plotted according to their spatial coordinates along the x-y axis (in pixels) with different colours representing the different clusters that they belong to. The ENS network starts as small clusters (3 dpf) and these clusters merge as development occurs. They start intermingling from 4 dpf onwards, finally span a longer length of the gut and bring about the waves of peristalsis.

3.3.3 Waves of peristalsis organise over development

The general approach, used in the host lab, to find sequences from neural data is to average across many trials and detect patterns. But this is only applicable for experiments where an animal receives a stimulus and the exact time-points for stimulus presentation are known. Since the data in this project captured spontaneous activity of the ENS neurons, it was difficult to have a sense of when to expect neural activity.

I used a toolbox called sequential non-negative matrix factorization (seqNMF) (Mackevicius et al., 2019). It detects temporal sequences and structure of these sequences from high dimensional neural activity data. Initially, it identifies repeating neural sequences (factors) and groups them according to the sequence in which they show peak activation over time. Further, the neurons are sorted according to the latency of their peak activation for each sequence (Figure 3.9). Each sequence found is represented in a different colour. On the left are the patterns that it detected (H) and the time courses (W) are shown on top. W shows the time-points at which each of these detected sequences occur.

This provides a glimpse of how the dynamics of the observed waves change over development. At 3 dpf (Figure 3.9 A), it is observed that three different sequences are detected for this larva where W3 seems to be preceding W2 sometimes while W1 seems to be occurring independently. For 4 dpf larva, (Figure 3.9 B), three sequences were detected. Amongst these, W1 seems to be occurring periodically. Comparing the occurrence of sequences detected at 4 dpf to those in 3 dpf, a transition towards structured activity is observed. Three different sequences are seen for a 5 dpf larva (Figure 3.9 C), with all three occurring at regular intervals and approximately equally contributing to the total activity. These three detected sequences seem to be showing a certain temporal pattern in which they fire. W2 precedes W1 while these occur at regular intervals. For a 6 dpf larva (Figure 3.9 D), only one sequence is detected, which seems to be occurring very periodically and frequently. For a 7 dpf larva (Figure 3.9 E), two sequences are detected out of which W2 occurs very periodically and keeps occurring continuously. In summary, at 3 dpf, the ENS network activity involves many unorganised and random bouts of different sequences contributing to the overall activity. At 4 dpf, the activity slowly starts organising and periodicity sets in. From 5 dpf onwards, it takes shape and the observed sequences seem to be organised in a very periodic manner. As

development progresses, from 6 dpf onwards, this periodicity persists with mostly one sequence generally dictating most of the activity that is seen in the ENS.

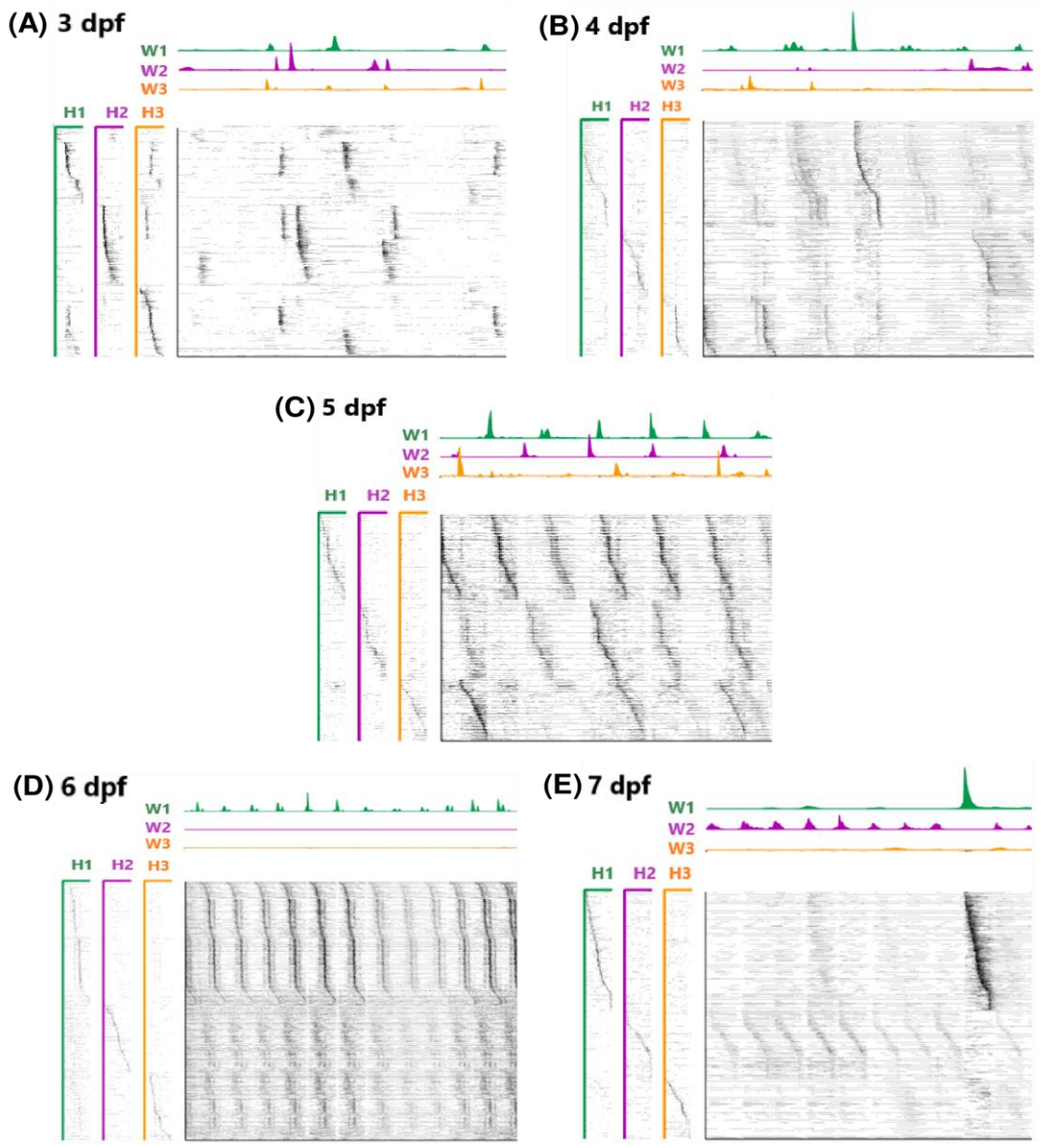

Figure 3.9 Waves of peristalsis evolve over development. On the left, Hs are the patterns detected by seqNMF and on top, Ws are the time courses over which they occur. Random sequences are observed at 3 dpf. From 4 dpf onwards, well structured, periodic sequences are observed.

I next mapped the ROIs giving rise to the sequences (Figure 3.10) spatially onto their coordinates and represented them with a temporal colour code (Figure 3.10). The ROIs giving rise to each sequence are shown in a separate image. Events occurring earlier in time are represented in lighter colours and the ones later are represented in darker colours. In a 3 dpf larva (Figure 3.10 A), the sequences W1 and W2 are restricted to specific areas of the gut. W1 spans a smaller area

towards the caudal end and W2 spans most of the central and rostral end. The W3 sequence occurs all over the gut. For a 4 dpf larva (Figure 3.10 B), many more neurons participate in the sequences as compared to 3 dpf and these sequences span almost the entire posterior gut. The gradient of colours that is observed indicates that the neurons fire sequentially and work towards forming the waves. In a 5 dpf larva (Figure 3.10 C), more continuous gradients are observed. In the images showing W1 and W2, two different waves are captured. In 6 and 7 dpf larvae (Figure 3.10 D and E respectively), smooth gradients are observed representing the waves that arise and spread from rostral to caudal direction.

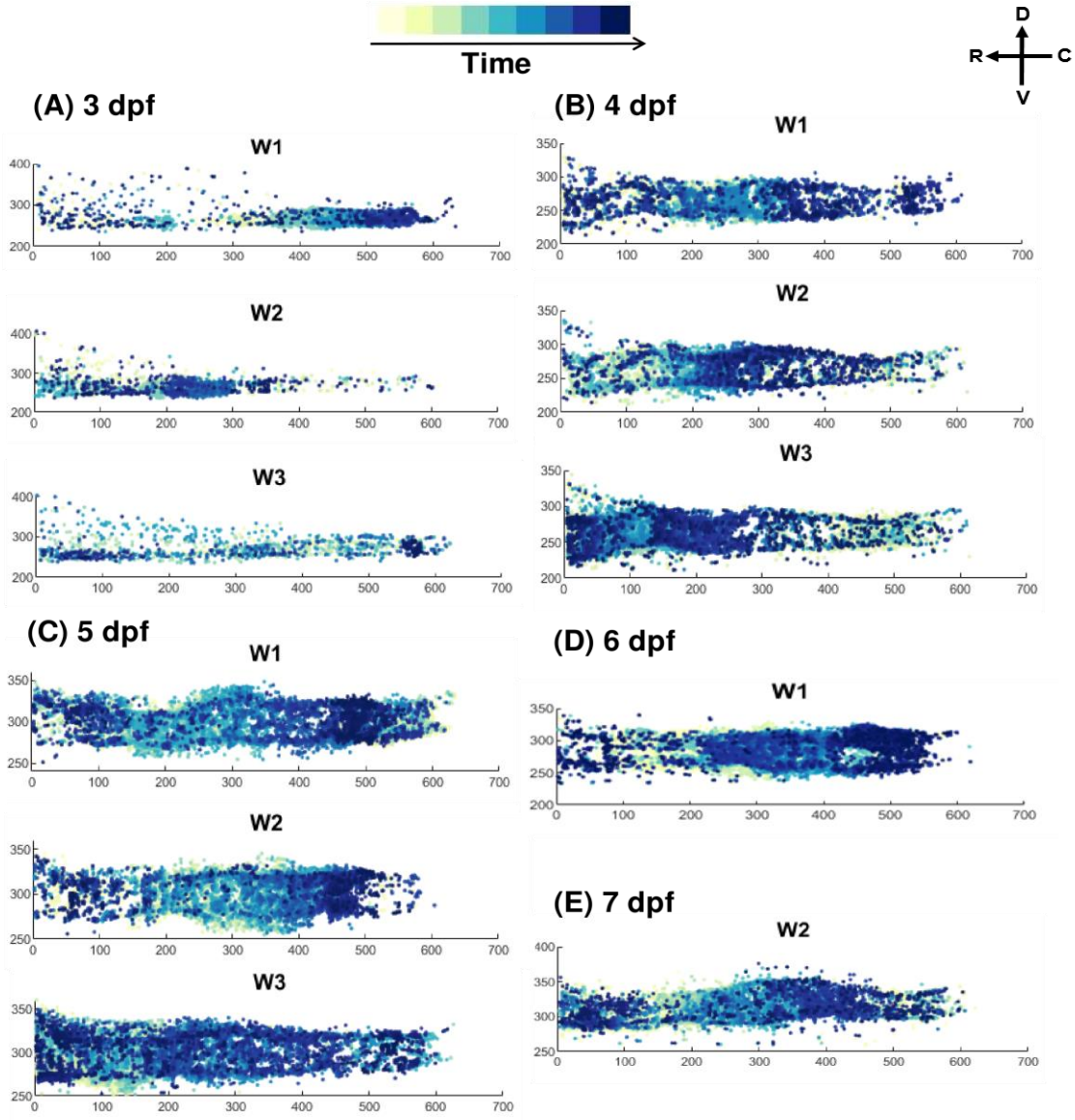

Figure 3.10: Waves of peristalsis organise over development. ROIs giving rise to the sequences detected by seqNMF (Figure 3.5) were mapped onto their spatial coordinates along the x-y axis (in pixels). A 2D plot was created wherein these ROIs where represented with a temporal colour code according to their latency (A-E).

3.4 Serial block face scanning electron microscopy (SBFSEM)

To investigate the anatomy of the neural network architecture of the ENS, we ran a fast trial of serial block face scanning electron microscopy on a 5 dpf larval zebrafish with a nominal sectioning thickness of 50 nm and 4096 x 3530 voxels at 50nm resolution. The SBFSEM images captured different components of the gut and ENS such as enteroendocrine cells (red) lining it and neurons and glia (green) that innervate it (Figure 3.8 A). The size of the gut varied across depth (Figure 3.11 B-G). However, we have not analysed the data yet. This will be done using image segmentation tools like Vaa3D, TrackEM2 or deep learning based approaches (Urakubo et al., 2019, Haberl et al., 2018).

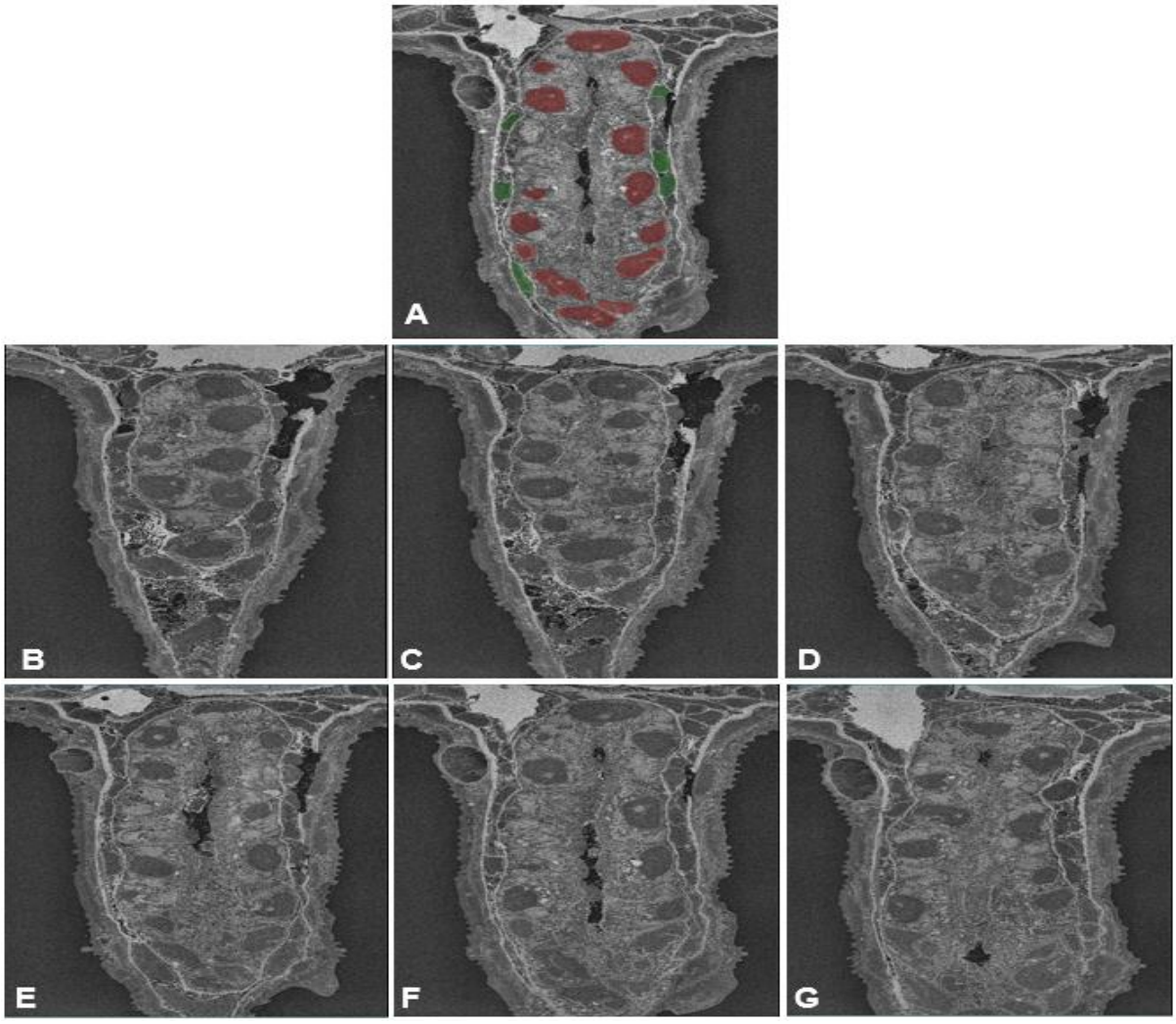

Figure 3.11: SBFSEM of a 5 dpf zebrafish gut. (A) Cells lining the gut are shown in red and the neurons innervating it are shown in green. (B-G) Snapshots of the gut at different depths.

Chapter 4
Discussion

In this study, I investigated the functional development of the ENS in larval zebrafish in vivo, using light-sheet microscopy. The major aim has been to characterize the growth of the ENS network and its activity to gain insights into the dynamics of this process. I employed a bioinformatics pipeline developed in our lab to pre-process the obtained calcium imaging data and analysed the neural data to delve into the various aspects of development of the ENS network.

The ENS network shows substantial changes over the course of its early development. There was no enteric innervation at 2 dpf. But it is also necessary to mention that the results presented here are only from the data from the posterior gut as I did not have the time to analyse the midgut data that I collected. There is also a possibility that at 2 dpf, only the mid-gut is innervated by enteric neurons as the ENS starts forming from the anterior part of the gastrointestinal axis and progresses towards the posterior end. Analysing the data from the mid-gut will help understand this and also give more insights about the development of the ENS.

The ENS neurons grow in number from 3 to 5 dpf and afterward decrease at 6 and 7 dpf. The activity of these neurons increases from 3 to 6 dpf and goes back to low at 7 dpf. Thus, the number of neurons and activity, both show a decline around 6 and 7 dpf. This could be because over development, anatomical pruning and wiring of the network might be eliminating certain neurons from the network. So in the early stages (3 and 4 dpf), when the network just starts forming, the neurons might be in their wiring or training phase. Subsequent pruning and refinement as a part of the network's development can be an explanation for the decline in number and activity of the ENS neurons that I observed. This decline of spontaneous activity after 5-6 dpf has also been observed during the development of the zebrafish tectum and is also shown to be driven by visual experience (Avitan et al., 2017). The fact that the activity can also be driven by experience leads us to the next plausible reason for the decline in activity that is observed. In their early life, zebrafish are dependent on their yolk sac for their nutritional requirement. They only start feeding from 5 or 6 dpf. The 7 dpf time-point, at which a decline in activity is observed also happens to be the

time when their yolk sac is completely used up and exogenous feeding becomes essential. There is a possibility that the ENS activity could be modulated by food, which we are planning to study next. The observed decline in activity could just be because the lack of exogenous food to process down regulates activity. This can be tested by doing experiments in fed larvae and comparing them to unfed ones.

The number of gut ROIs extracted from pre-processing goes to about 50,000. This is way higher than the actual biologically plausible number of neurons expected in the gut. It is because the ROIs were extracted from individual x-y slices that were captured 5 µm apart. This led to over segmentation and the same ROI was extracted multiple times from different subsequent slices because CaImAn does not perform 3D segmentation. This can be improved by using a maximum intensity projection in z-axis across time stack to extract ROIs or by using a 3D segmentation tool. However, even after correcting the over segmentation, I expect that the trend observed in the number of ROIs over development will continue to be the same. This is because in this case, the overall number of ROIs should be reduced consistently across all ages.

Spontaneous waves of depolarisation are observed starting from 3 dpf, similar to what is observed by Holmberg et al., 2004. These are representative of the waves of peristalsis that are brought about by the ENS. At 3 dpf, the waves seemed to be sporadic with no particular pattern to them. These tend to travel in the anterograde direction (from rostral to caudal) along the posterior gut or start in the middle and traverse both ways. Starting 4 dpf, more organised, regular and coordinated wave patterns are observed where they generally tend to travel in the anterograde direction. The neural activity was correlated at 3 and 4 dpf and over development, as the waves became robust, the correlation between neurons declined. This was not what I initially expected. I expected the correlation between neurons to increase as the waves get more coordinated over development. However, the decrease in correlation that is seen might be because as the waves become more organised and traverse longer lengths of the gut, it is important that certain groups of neurons need to stop firing at the same time as certain adjacent group of neurons participating in the wave are firing. However, this decreased correlation seems to be more like only an observed trend and needs to be addressed further in order to conclusively infer

what is happening. The next step would be to employ a correlation based graph theory approach to visualize the groups of neurons that fire simultaneously.

The sequences of neural activity giving rise to these waves were dissected from the data using seqNMF. Early in development (3 dpf), many different sequences are seen to be equally involved in the observed activity in a sporadic manner. They are generally restricted to certain regions of the posterior gut. From 4 dpf, the sequences start becoming more structured and regular. Following this, from 5 – 6 dpf onwards, more disciplined patterns of sequences are observed. However, this is my interpretation of the seqNMF plots that were obtained for individual larvae. In order to ensure that the phenomenon being observed is present in all individual animals within a group, it is necessary to combine data from multiple animals. The next step would be to quantify the observed sequences by calculating their frequency and velocity for every larva based on seqNMF. The data from these parameters can be combined from multiple animals within groups. A few fishes also seemed to deviate from this general trend and were slightly ahead or back in terms of the activity for that particular age. This may be due to differences in individual development. A t-SNE analysis was employed using correlation as a distance and further, clusters of neurons were identified and visualized over development. This analysis indicates that the ENS neuronal network starts out as micro circuits with random activity, which slowly merge over development and bring about well-organised waves of peristalsis spanning larger areas of the gut.

In summary, the ENS network follows a unique developmental trajectory and exhibits waves of peristalsis that evolve over time and prepare to bring about gut motility before external feeding starts.

Chapter 5
Conclusion

In this project, I characterized the ontogeny of the ENS network development and its activity in larval zebrafish. The ENS network follows a specific developmental trajectory wherein the functional architecture grows till 5 dpf and declines from there until 7 dpf. At 3 dpf, the ENS neurons are low in number and exhibit random firing patterns. Further in development, they increase in number until 5 dpf and decline from 6 to 7 dpf. The neural activity increases from 3 dpf to 6 dpf. At 7 dpf, the activity declines and becomes comparable to that observed at 3 dpf. The ENS network starts out as multiple microcircuits with gradually increasing, random activity. As development progresses, these microcircuits start intermingling and merging to form larger circuits, and ultimately spread along the gut with overall coordinated activity bringing about waves of peristalsis. These waves are formed by firing sequences orchestrated by groups of neurons. Sporadic activity is present at 3 dpf where many different sequences contribute randomly to the observed activity. These travel from rostral to caudal direction as well as in the opposite direction. From 4 dpf onwards, this activity becomes coordinated, giving rise to waves that mostly travel from rostral to caudal direction. Thus, the ENS activity is sporadic at early developmental time-points (3 dpf) and further shapes into organised and coordinated activity patterns as development progresses. These findings give a glimpse of the early functional development of the ENS in larval zebrafish and lay the basis for exciting avenues of future work.

Chapter 6
Future directions

The ENS neural activity needs to be dissected in more details to get deeper and firm insights into its functional development. It can be further characterized by quantifying the properties such as velocity and frequency of observed waves of peristalsis. Graph theory can be employed to analyse the networks or clusters of neurons that show similar characteristics (correlation based). The density of the network over development can be evaluated by calculating the average distance between ROIs. Experiments with fed animals will prospectively help provide a conclusive reason behind the lowered activity that I observed at 7 dpf. The SBFSEM analysis will help understand the anatomical architecture of the ENS.

The findings from this project further direct us towards interesting prospective studies. The ENS development and activity can be characterized in germ-free larvae. This will serve as a basis to study the influence of the gut microbiome on the development of ENS. Comparing the ENS network activity properties between wild-type and germ-free larvae will help us understand the developmental factors that are influenced by the microbiome. This will also pinpoint the critical time-points at which gut microbiome is essential for ENS development. The germ-free approach can be applied to disease models such as autism spectrum disorder mutants. This will shed light on how the gut microbiome influences ENS development in disease models, and most importantly it will help establish causal links about the influence of gut microbiome on ENS development.

Chapter 7
References

1. Adams, J.B., Johansen, L.J., Powell, L.D., Quig, D., and Rubin, R.A. (2011). Gastrointestinal flora and gastrointestinal status in children with autism - comparisons to typical children and correlation with autism severity. BMC Gastroenterol. *11*, 22.
2. Arseneault-Bréard, J., Rondeau, I., Gilbert, K., Girard, S.A., Tompkins, T.A., Godbout, R., and Rousseau, G. (2012). Combination of Lactobacillus helveticus R0052 and Bifidobacterium longum R0175 reduces post-myocardial infarction depression symptoms and restores intestinal permeability in a rat model. Br. J. Nutr. *107*, 1793–1799.
3. Asano, Y., Hiramoto, T., Nishino, R., Aiba, Y., Kimura, T., Yoshihara, K., Koga, Y., and Sudo, N. (2012). Critical role of gut microbiota in the production of biologically active, free catecholamines in the gut lumen of mice. Am. J. Physiol. Gastrointest. Liver Physiol. *303*, 1288–1295.
4. Avitan, L., Pujic, Z., Mölter, J., Van De Poll, M., Sun, B., Teng, H., Amor, R., Scott, E.K., and Goodhill, G.J. (2017). Spontaneous Activity in the Zebrafish Tectum Reorganizes over Development and Is Influenced by Visual Experience. Curr. Biol. *27*, 2407–2419.e4.
5. Barrett, E., Ross, R.P., O'Toole, P.W., Fitzgerald, G.F., and Stanton, C. (2012). γ-Aminobutyric acid production by culturable bacteria from the human intestine. J. Appl. Microbiol. *113*, 411–417.
6. Bercik, P., Denou, E., Collins, J., Jackson, W., Lu, J., Jury, J., Deng, Y., Blennerhassett, P., MacRi, J., McCoy, K.D., et al. (2011). The intestinal microbiota affect central levels of brain-derived neurotropic factor and behavior in mice. Gastroenterology *141*, 599–609.
7. Borre, Y.E., O'Keeffe, G.W., Clarke, G., Stanton, C., Dinan, T.G., and Cryan, J.F. (2014). Microbiota and neurodevelopmental windows: implications for brain disorders. Trends Mol. Med. *20*, 509–518.
8. Bravo J.A., Forsythe P., Chew M.V., Escaravage E., Savignac H.M., Dinan T.G., Bienenstock J., Cryan J.F. (2011). Ingestion of Lactobacillus strain regulates

emotional behavior and central GABA receptor expression in a mouse via the vagus nerve. Proc. Natl. Acad. Sci. U S A *108,* 16050–16055.

9. Chaidez V, Hansen RL, Hertz-Picciotto I. (2014). Gastrointestinal problems in children with autism, developmental delays or typical development. J Autism Dev Disord *44*:1117-1127.
10. Chen, T.W., Wardill, T.J., Sun, Y., Pulver, S.R., Renninger, S.L., Baohan, A., Schreiter, E.R., Kerr, R.A., Orger, M.B., Jayaraman, V., et al. (2013). Ultrasensitive fluorescent proteins for imaging neuronal activity. Nature *499*, 295–300.
11. Constantin, L., Poulsen, R.E., Favre-Bulle, I.A., Taylor, M.A., Sun, B., Goodhill, G.J., Vanwalleghem, G.C., and Scott, E.K. (2019). Altered brain-wide auditory networks in fmr1-mutant larval zebrafish. BioRxiv 722082.
12. Crumeyrolle-Arias, M., Jaglin, M., Bruneau, A., Vancassel, S., Cardona, A., Daugé, V., Naudon, L., and Rabot, S. (2014). Absence of the gut microbiota enhances anxiety-like behavior and neuroendocrine response to acute stress in rats. Psychoneuroendocrinology *42*, 207–217.
13. Cryan, J.F., and Dinan, T.G. (2012). Mind-altering microorganisms: The impact of the gut microbiota on brain and behaviour. Nat. Rev. Neurosci. *13*, 701–712.
14. Desbonnet, L., Clarke, G., Shanahan, F., Dinan, T.G., and Cryan, J.F. (2014). Microbiota is essential for social development in the mouse. Mol. Psychiatry *19*, 146–148.
15. Desbonnet, L., Clarke, G., Traplin, A., O'Sullivan, O., Crispie, F., Moloney, R.D., Cotter, P.D., Dinan, T.G., and Cryan, J.F. (2015). Gut microbiota depletion from early adolescence in mice: Implications for brain and behaviour. Brain. Behav. Immun. *48*, 165–173.
16. Desbonnet, L., Garrett, L., Clarke, G., Bienenstock, J., and Dinan, T.G. (2008). The probiotic Bifidobacteria infantis: An assessment of potential antidepressant properties in the rat. J. Psychiatr. Res. *43*, 164–174.
17. Desbonnet, L., Garrett, L., Clarke, G., Kiely, B., Cryan, J.F., and Dinan, T.G. (2010). Effects of the probiotic Bifidobacterium infantis in the maternal separation model of depression. Neuroscience *170*, 1179–1188.
18. Edelstein, A., Amodaj, N., Hoover, K., Vale, R., and Stuurman, N. (2010). Computer control of microscopes using manager. Curr. Protoc. Mol. Biol. 1–22.
19. Friedrich, J., Zhou, P., and Paninski, L. (2017). Fast online deconvolution of calcium imaging data. PLOS Computational Biology *13*, e1005423.

20. Fülling, C., Dinan, T.G., and Cryan, J.F. (2019). Gut Microbe to Brain Signaling: What Happens in Vagus…. Neuron *101*, 998–1002.
21. Furness, J.B.; Callaghan, B.P.; Rivera, L.R.; Cho, H.J. (2014). The enteric nervous system and gastrointestinal innervation: Integrated local and central control. Advances in Experimental and Medicinal Biology *817*, 39–71.
22. Furness JB, Costa (1987). The enteric nervous system. (Churchill Livingstone, Edinburgh).
23. Ganz, J. (2018). Gut feelings: Studying enteric nervous system evelopment, function, and disease in zebrafish model system. Dev. Dyn. *247*, 268-278.
24. Giovannucci, A., Friedrich, J., Gunn, P., Kalfon, J., Brown, B.L., Koay, S.A., Taxidis, J., Najafi, F., Gauthier, J.L., Zhou, P., et al. (2019). CaImAn an open source tool for scalable calcium imaging data analysis. Elife *8*, 1–45.
25. Grunwald DJ, Eisen JS. (2002). Headwaters of the zebrafish - emergence of anewmodel vertebrate. Nat Rev Genet. *3*, 717–24.
26. Haberl, M.G., Churas, C., Tindall, L., Boassa, D., Phan, S., Bushong, E.A., Madany, M., Akay, R., Deerinck, T.J., Peltier, S.T., et al. (2018). CDeep3M—Plug-and-Play cloud-based deep learning for image segmentation. Nat. Methods *15*, 677–680.
27. Han, W., Tellez, L.A., Perkins, M.H., Perez, I.O., Qu, T., Ferreira, J., Ferreira, T.L., Quinn, D., Liu, Z.W., Gao, X.B., et al. (2018). A Neural Circuit for Gut-Induced Reward. Cell *175*, 665–678.e23.
28. Hao, M.M., Foong, J.P.P., Bornstein, J.C., Li, Z.L., Vanden Berghe, P., and Boesmans, W. (2016). Enteric nervous system assembly: Functional integration within the developing gut. Dev. Biol. *417*, 168–181.
29. Holmberg, A., Schwerte, T., Pelster, B., and Holmgren, S. (2004). Ontogeny of the gut motility control system in zebrafish Danio rerio embryos and larvae. J. Exp. Biol. *207*, 4085–4094.
30. Hsiao, E.Y., McBride, S.W., Hsien, S., Sharon, G., Hyde, E.R., McCue, T., Codelli, J.A., Chow, J., Reisman, S.E., Petrosino, J.F., et al. (2013). Microbiota modulate behavioral and physiological abnormalities associated with neurodevelopmental disorders. Cell *155*, 1451–1463.
31. Kaelberer MM, Buchanan KL, Klein ME, Barth BB, Montoya MM, Xiling Shen, Diego V. Bohórquez (2018). A gut-brain neural circuit for nutrient sensory transduction.Science*361*:eaat5236.

32. Kelly, J.R., Borre, Y., O' Brien, C., Patterson, E., El Aidy, S., Deane, J., Kennedy, P.J., Beers, S., Scott, K., Moloney, G., et al. (2016). Transferring the blues: Depression-associated gut microbiota induces neurobehavioural changes in the rat. J. Psychiatr. Res. *82*, 109–118.
33. Kulkarni, S., Ganz, J., Bayrer, J., Becker, L., Bogunovic, M., and Rao, M. (2018). Advances in enteric neurobiology: The "brain" in the gut in health and disease. J. Neurosci. *38*, 9346–9354.
34. Lyte, M., Cryan, J.F. (2014). Microbial endocrinology: The Microbiota-Gut-Brain axis in health and disease. Advancs in Experimental Medicine and Biology *817*, 3–24.
35. Mackevicius, E.L., Bahle, A.H., Williams, A.H., Gu, S., Denisenko, N.I., Goldman, M.S., and Fee, M.S. (2019). Unsupervised discovery of temporal sequences in high-dimensional datasets, with applications to neuroscience. Elife *8*, 1–42.
36. Ma, Q., Xing, C., Long, W., Wang, H.Y., Liu, Q., and Wang, R.F. (2019). Impact of microbiota on central nervous system and neurological diseases: The gut-brain axis. J. Neuroinflammation *16*, 1–14.
37. Matsumoto, M., Kibe, R., Ooga, T., Aiba, Y., Kurihara, S., Sawaki, E., Koga, Y., and Benno, Y. (2012). Impact of intestinal microbiota on intestinal luminal metabolome. Sci. Rep. *2*, 1–10.
38. Mayer, E.A. (2011). Gut feelings: The emerging biology of gut-brain communication. Nat. Rev. Neurosci. *12*, 453–466.
39. Mayer, E.A., Padua, D., and Tillisch, K. (2014). Altered brain-gut axis in autism: Comorbidity or causative mechanisms? BioEssays *36*, 933–939.
40. McDonald, D., Hyde, E., Debelius, J.W., Morton, J.T., Gonzalez, A., Ackermann, G., Aksenov, A.A., Behsaz, B., Brennan, C., Chen, Y., et al. (2018). American Gut: an Open Platform for Citizen Science Microbiome Research. MSystems *3*, 1–28.
41. McElhanon, B.O., McCracken, C., Karpen, S., and Sharp, W.G. (2014). Gastrointestinal symptoms in autism spectrum disorder: A meta-analysis. Pediatrics *133*, 872–883.
42. Mertsalmi, T.H., Aho, V.T.E., Pereira, P.A.B., Paulin, L., Pekkonen, E., Auvinen, P., and Scheperjans, F. (2017). More than constipation – bowel symptoms in Parkinson's disease and their connection to gut microbiota. Eur. J. Neurol. *24*, 1375–1383.
43. Neufeld, K.M., Kang, N., Bienenstock, J., and Foster, J.A. (2011). Reduced anxiety-like behavior and central neurochemical change in germ-free mice.

Neurogastroenterol. Motil. *23*.

44. Obata, Y., and Pachnis, V. (2016). The Effect of Microbiota and the Immune System on the Development and Organization of the Enteric Nervous System. Gastroenterology *151*, 836–844.
45. Petschow, B., Doré, J., Hibberd, P., Dinan, T., Reid, G., Blaser, M., Cani, P.D., Degnan, F.H., Foster, J., Gibson, G., et al. (2013). Probiotics, prebiotics, and the host microbiome: The science of translation. Ann. N. Y. Acad. Sci. *1306*, 1–17.
46. Pnevmatikakis, E.A., and Giovannucci, A. (2017). NoRMCorre: An online algorithm for piecewise rigid motion correction of calcium imaging data. J. Neurosci. Methods *291*, 83–94.
47. Rao, M., and Gershon, M.D. (2016). The bowel and beyond: The enteric nervous system in neurological disorders. Nat. Rev. Gastroenterol. Hepatol. *13*, 517–528.
48. Singh, V., Roth, S., Llovera, G., Sadler, R., Garzetti, D., Stecher, B., Dichgans, M., and Liesz, A. (2016). Microbiota dysbiosis controls the neuroinflammatory response after stroke. J. Neurosci. *36*, 7428–7440.
49. Sommer, F., and Bäckhed, F. (2013). The gut microbiota-masters of host development and physiology. Nat. Rev. Microbiol. *11*, 227–238.
50. Sudo, N., Chida, Y., Aiba, Y., Sonoda, J., Oyama, N., Yu, X.N., Kubo, C., and Koga, Y. (2004). Postnatal microbial colonization programs the hypothalamic-pituitary-adrenal system for stress response in mice. J. Physiol. *558*, 263–275.
51. Taylor, C.R., Montagne, W.A., Eisen, J.S., and Ganz, J. (2016). Molecular fingerprinting delineates progenitor populations in the developing zebrafish enteric nervous system. Dev. Dyn. *245*, 1081–1096.
52. Taylor, M.A., Vanwalleghem, G.C., Favre-Bulle, I.A., and Scott, E.K. (2018). Diffuse light-sheet microscopy for stripe-free calcium imaging of neural populations. J. Biophotonics *11*, 1–9.
53. Tolhurst G., Heffron H., Lam Y.S., Parker H.E., Habib A.M., Diakogiannaki E., Cameron J., Grosse J., Reimann F., Gribble F.M. Short-chain fatty acids stimulate glucagon-like peptide-1 secretion via the G-protein-coupled receptor FFAR2. Diabetes.
54. Urakubo, H., Bullmann, T., Kubota, Y., Oba, S., and Ishii, S. (2019). UNI-EM: An Environment for Deep Neural Network-Based Automated Segmentation of Neuronal Electron Microscopic Images. Sci. Rep. *9*, 1–9.

55. Valles-Colomer, M., Falony, G., Darzi, Y., Tigchelaar, E.F., Wang, J., Tito, R.Y., Schiweck, C., Kurilshikov, A., Joossens, M., Wijmenga, C., et al. (2019). The neuroactive potential of the human gut microbiota in quality of life and depression. Nat. Microbiol. *4*, 623–632.
56. Vuong, H.E., and Hsiao, E.Y. (2017). Emerging Roles for the Gut Microbiome in Autism Spectrum Disorder. Biol. Psychiatry *81*, 411–423.
57. Wallace, K.N., Akhter, S., Smith, E.M., Lorent, K., and Pack, M. (2005). Intestinal growth and differentiation in zebrafish. Mech. Dev. *122*, 157–173.
58. Wang, Y., Telesford, K.M., Ochoa-Repáraz, J., Haque-Begum, S., Christy, M., Kasper, E.J., Wang, L., Wu, Y., Robson, S.C., Kasper, D.L., et al. (2014). An intestinal commensal symbiosis factor controls neuroinflammation via TLR2-mediated CD39 signalling. Nat. Commun. *5*, 1–10.
59. Wang, Z., Du, J., Lam, S.H., Mathavan, S., Matsudaira, P., and Gong, Z. (2010). Morphological and molecular evidence for functional organization along the rostrocaudal axis of the adult zebrafish intestine. BMC Genomics *11*.
60. Ye, L., & Liddle, R. A. (2017). Gastrointestinal hormones and the gut connectome. Current opinion in endocrinology, diabetes, and obesity, *24*(1), 9–14.
61. Zheng, P., Zeng, B., Zhou, C., Liu, M., Fang, Z., Xu, X., Zeng, L., Chen, J., Fan, S., Du, X., et al. (2016). Gut microbiome remodeling induces depressive-like behaviors through a pathway mediated by the host's metabolism. Mol. Psychiatry *21*, 786–796.